Final Report

Contract: 87055-15-0226-1
Assessment of RELAP5 for Natural Circulation

McMaster University

To:

Dan Simard
Senior Contracting Officer
CNSC

Christine Howden
Research Program Officer
CNSC

Prepared by:

Kendall Boniface
Feng Zhou

Principal Investigator:

D.R. Novog
Professor
McMaster University
Department of Engineering Physics
1280 Main St. West, Hamilton, Ontario

Date: March 28, 2017

Contents

List of Tables

List of Figures

1. Introduction

A fundamental safety objective in a nuclear reactor is to ensure sufficient cooling of the fuel at all times. In any reactor design the primary heat transport system provides the necessary means for transporting heat from the fuel to the heat sink. This system is specifically designed to be capable of adequate core heat removal under both normal operating conditions and a wide range of postulated shutdown and accident conditions. During normal operation, the primary heat transport system (PHTS) pumps provide forced circulation to remove heat from the core and deposit it in the steam generators (SG). However, it is possible under certain accident conditions that forced circulation may be lost and natural circulation is required for the removal of decay heat. Natural circulation may provide cooling for a significant period of time, however depending on the state of the core during the accident, the SG secondary-side inventory may be depleted, requiring operator actions to ensure the viability of the heat sink. In order for these operator actions to be beneficial, it is necessary to base them on an in-depth understanding of the progression of physical phenomena that can occur under these conditions.

There are several modes of natural circulation: one- and two-phase thermosyphoning, intermittent buoyancy induced flow (IBIF) and continuous steam venting. It is important to understand and predict the phenomena and associated fuel and pressure tube (PT) temperatures during each mode of natural circulation in order to ensure that all parameters remain within acceptable safety limits. Currently the prediction of these natural circulation heat sinks are performed using a variety of tools developed specifically for CANDU designs (e.g. CCAFF – Core Cooling in the Absence of Forced Flow). The Reactor Excursion and Leak Analysis Program (RELAP5) is an internationally available one-dimensional transient thermalhydraulic network simulation code that is widely used in the nuclear industry. It is part of the US NRC CAMP code project and hence has a wide basis of use and validation. While some effort has been spent to adopt the standard RELAP5 models to the horizontal pressure tube design of the CANDU reactor, the accuracy of the code under natural circulation scenarios has not previously been established.

In particular, RELAP5 predictions of the IBIF mode of natural circulation require further study given that a vast majority of studies using RELAP focus on vertically oriented fuel channels. After initial stagnation in a fuel channel, the heat transport system coolant within the channel will heat up to saturation and boil. As a void grows within a CANDU channel during IBIF, fuel elements at the top of each channel will be exposed to vapour. The cladding-to-vapour heat transfer rate is significantly lower than the cladding-to-liquid rate, causing these uncovered elements to experience significantly higher rates of temperature increase. A further complexity under these conditions is that although the steam and liquid remain largely separated, the boiling within the liquid portion will tend to generate wet steam (i.e., steam with a quality of less than 100%). Furthermore, unlike axial flows that are typical in many simulations using system thermalhydraulic codes, the transport of vapour and liquid droplets in this circumstance is lateral across the bundle (since the flow is stagnated). Hence liquid entrainment within the steam section of the channel may be significant. As such the amount of thermal non-equilibrium that can occur is limited by the presence of liquid droplets in the steam. Such a mixture of droplet-rich steam would also tend to yield much higher heat transfer coefficients relative to pure steam cooling. Such phenomena are clearly evident in the available experiments which show that the top-most fuel elements while at a high temperature, do not exhibit pure steam-like heatup.

When the growing void has extended from the channel to the corresponding feeder connection the low-density steam is able to vent through the feeder to the higher-elevation header, pulling cooler water into the channel from the opposite feeder and header. In a full-scale CANDU system, venting in a single channel may or may not create a sufficient imbalance in the header pressures to initiate venting in all channels in a given core pass, however in most full-scale experimental tests the perturbations from a single-channel venting is enough to initiate venting in other channels. It is important to accurately predict the amount of time that fuel elements will remain in contact with vapour and their associated maximum temperatures in order to ascertain whether the material failure limit will be reached by any components. The objective of this research has been to quantify the capability of RELAP5 for predictions of the thermalhydraulic behaviour that occurs in a CANDU channel undergoing the IBIF mode of natural circulation.

2. Summary of Work Plan

This project examined the theoretical and empirical models within RELAP for applicability to a CANDU IBIF cycle. Validation of RELAP5 was performed based on available experimental data from the series of standing-start tests performed at the full-scale Cold Water Injection Test (CWIT) Facility. The experimental facility and imposed thermalhydraulic conditions were modeled within the RELAP5 architecture and the results were compared with those from the test facility. This report presents an examination of the relevant physical phenomena, the corresponding correlations implemented within the code, and a detailed analysis of the resulting thermalhydraulic predictions.

3. Background Information

Natural circulation driven heat removal from the core may occur under a variety of conditions. The most frequently encountered is continuous single-phase or two-phase thermosyphoning wherein buoyancy forces drive the lower density liquid in the core upwards to the steam generator and cold liquid is drawn through the core. Under such circumstances flows typically are unidirectional in a core pass and do not exhibit large fluctuations or changes in direction. It is possible under certain conditions for continuous natural circulation to break down causing flow stagnation within the channels. Several possible scenarios of this type are listed below:

1) A reduction in the inventory of the primary heat transport system may preclude continuous natural circulation from the core to the steam generator due to the lack of a continuous flow path around the loop. Alternatively a large amount of non-condensable gases may also preclude continuous natural circulation.
2) If the secondary side is rapidly depressurized during an operator initiated crash-cool, the temperature in the steam generator will drop significantly. Such a drop in the secondary side temperatures will cause an increase in heat removal from the primary side. With no inventory make-up, the primary side will also depressurize due to shrinkage of the HTS inventory. A situation will arise where both the primary and secondary sides are both near saturation at similar temperatures. Under such conditions buoyancy forces may not be sufficient to sustain continuous flow.

While the HTS flows may temporarily stagnate in these scenarios, there still exists a large potential for heat deposition to the secondary side of the steam generator (or through reflux condensation and or/containment venting if the HTS is open during an outage) through IBIF phenomena.

IBIF occurs in a series of phenomenological stages:

1) Channel stagnation
2) Channel heatup
3) Void or hot slug growth
4) End-fitting penetration
5) Venting

From a standing start condition (i.e., channel flow stagnation), the coolant in the channel is continuously heated with the potential formation of a vapour bubble beginning in the middle of the channel and growing outward to the end-fittings. Void initiates and grows from the center of the channel since decay heat follows a similar profile as the power distribution prior to shut-down. With continued vapour generation the bubble will grow in height, exposing some fuel pins to steam, and length, extending towards the end-fittings. The end-fittings consist of a large amount of metal that is initially at a significantly lower temperature than the stagnated coolant. As such, when void begins to penetrate the end-fittings the vapour will continuously condense until the mass of metal has reached the saturation temperature. When the void has penetrated far enough into the end-fitting that it has reached the connection to the feeder, the combined buoyant force and availability of flow path allows the entire void to exit the channel through the feeder toward the header. When this occurs, the pressure distribution in the system because favorable and flow is initiated from the opposite side of the channel. This flow is temporary and ceases once the entire pocket of void reaches the header, however, during this time the coolant is replenished in the channel and the fuel is cooled. Flow eventually stagnates again and the process may repeat. Such cycles may repeatedly occur as long as sufficient inventory remains to replenish the void released from the channel.

The concern during the IBIF cycle is the prolonged presence of significant void within the channel. During these conditions it is possible for fuel elements and top of the pressure tube to be exposed to steam for an extended period of time. As a direct consequence of this, demonstrating the effectiveness of IBIF as a suitable heat sink requires establishing that the venting time and the associated maximum fuel sheath and pressure tube temperatures are well within the allowable safety limits.

4. Literature Review

4.1 Intermittent Buoyancy-Induced Flow

Intermittent Buoyancy Induced Flow (IBIF) is a unique phenomenon in CANDU reactors which have horizontal fuel channels, vertical feeders and steam generators at high elevation relative to the core. IBIFs have been observed experimentally, e.g. in the RD-14M tests [1], in the CWIT facility tests [2], and other experiments [3]. While many code validation activities have been performed, a majority of these are within protected industry documentation, the review below presents the information available in the open literature.

A large number of experimental tests have been conducted in integral CANDU thermalhydraulic test loops, i.e. RD-14M facility, on both single-phase and two phase natural circulation. The descriptions and results of test series R (i.e. transition from forced circulation to thermosyphoning) and test series T (i.e. transition from thermosyphoning to other natural circulation modes) are available from open literature [1] [4]. These tests cover a wide range of conditions with power ranging from 60 to 160kW/pass, and secondary side pressures from 0.1 to 4.5 MPa (g). For test series T, single phase natural circulation was established prior to the transient. Then the primary side inventory was reduced through a series of discrete drains from the header. Some of the important findings were:

1) With the decrease in HTS inventory the primary-side flow rate increased as single phase natural circulation transitioned into two phase mode. Eventually the maximum flow rate (through the steam generator) was reached and further reduction in HTS inventory led to the decrease in flow rate and flow reversal in some of the fuel channels. Channels at higher elevation were more likely to experience flow reversal.
2) The breakdown of unidirectional natural circulation did not cause a simultaneous breakdown in core or channel cooling. Bidirectional flow in the fuel channels and reflux condensation in the boiler become the effective and prime heat rejection mechanisms at lower inventories.
3) For the majority of tests the Fuel Element Simulator (FES) did not heat up until primary fluid inventories were reduced to less than 70%.
4) Only in a small subset of tests, FES heatup occurred at primary fluid inventories greater than 85%, and was attributed to void penetration of the inflow feeder (VPIF) phenomenon.

Lei et al. [5] assessed the fuel fitness-for-service after repeated IBIF cycles during a maintenance outage at Gentilly 2 assuming both the steam generator and shutdown cooling system are unavailable. They first defined a number of criteria for the fuel bundles and pressure tubes to return to service. The number of IBIF cycles, coolant temperature and heatup times in each IBIF cycle were calculated using code THERMOSS-III. The results were then used by HOTSPOT to calculate the transient pressure tube temperature and heat transfer coefficient from fuel to steam. ELESTRES was used to generate initial conditions for the fuel. The results calculated by the above three codes were then used by ELOCA.Mk6 to assess the thermal-mechanical behavior of fuel element. With a fuel sheath limiting temperature of 450^{o}C and pressure tube limiting temperature of 400^{o}C their results showed that the fuel channel is suitable for returning to full power after repeated IBIF cycles. Such analysis shows that for very low decay heat levels typical of a maintenance outage the fuel channel can survive extended periods where forced flow may be unavailable.

The IBIFs in the CWIT experiments have been simulated using the thermalhydraulic code GOTHIC [6]. Simulations were carried out for both the symmetrical and asymmetrical channel configurations. It was found that for single-phase IBIF, the impact of partial obstructions in one of the channel is not prohibitive. For two-phase IBIF, computational demands precluded the completion of two-phase simulations in a reasonable timeframe using GOTHIC; however useful insights and observations are drawn from the early stages that are successfully simulated:

1) The heat-up of pin prior to the exposure to vapour was reasonably predicted.
2) After pin exposure, the model predicted an approximately adiabatic heatup rate, while the temperature of the pins in the CWIT experiment increased more slowly, suggesting that some froth or spray was present throughout the steam in the experiment.
3) A projection of the end fitting temperature suggested that the model would over-predict venting time if the simulation were to run to completion.

Karchev et al. [3] conducted an experiment using air and water at atmosphere pressure to quantitatively study the IBIF phenomena. The pressure tube was represented by 9m long acrylic tube. Two vertical tubes simulating the feeder pipes are attached at the ends of test channel with the other end connected to two open water tanks. Air bubbles were injected into the horizontal tube at various axial locations to simulate vapor generation. Their results showed that an increase in the water level in the feeder pipes and the decrease in power level (lower air injection rate) resulted in the increase in the venting time. It was also found a small amount of sag in the pressure tube could cause a significant decrease in venting time.

4.2 Flow Regime Maps in RELAP5

4.2.1 The Horizontal Flow Regime Map

RELAP5 uses a two-dimensional flow regime map for horizontal flow. First, it determines whether the flow is horizontally stratified, non-stratified, or a mixture of the two. If the flow is not horizontally stratified, then it is either bubbly, slug, annular mist, or mist, or a transitional flow regime, depending on the void fraction.

Traditional flow regime maps would use liquid and vapour superficial velocity, but analysis by Ishii and Mishima shows that such mappings are very weak except under steady-state, fully-developed flow conditions. The mappings used by RELAP5 thus use void fraction as a primary variable, along with other variables to determine flow regimes. While these flow regime maps are still validated mainly for steady-state, fully-developed flows, but they provide more suitable results for transient and entrance conditions than traditional flow regime maps [7].

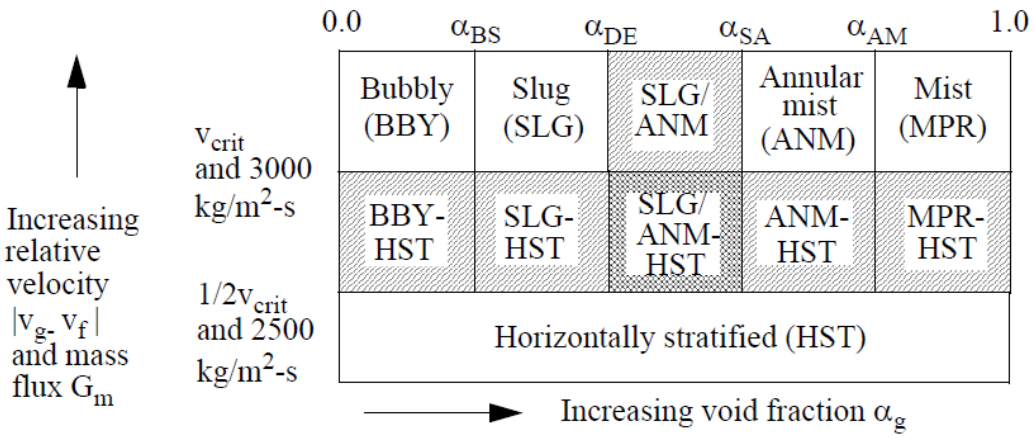

Figure 1 Flow regime map plot for horizontal pipes in RELAP5 [7]

The primary criterion on the vertical axis is Kelvin-Helmholtz instability as given by Taitel and Dukler, which has been validated against Mandhane et al.'s flow regime map, and is similar to the weighting factor W_2 in CATHENA. The critical velocity v_{crit}, however, is of a different form [7]:

$$v_{crit} = \frac{1}{2}\sqrt{\frac{(\rho_f - \rho_g) g \alpha_g A}{\rho_g D \sin\theta}}(1 - \cos\theta) \quad (1)$$

Where θ is the polar angle between the vertical and the fluid interface (see Figure 2 below):

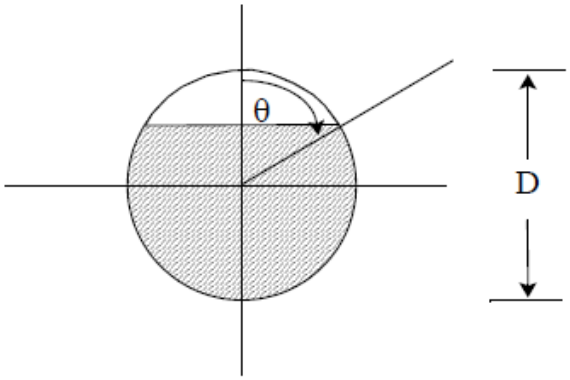

Figure 2 Convention for the collapsed liquid level term in RELAP5 [7]

The secondary criterion is the mass flux G_m, so that stratified flow is prohibited under high flow conditions. An additional criterion provides a smooth transition from stratified to mixed flow for gas velocities between 10 m/s and 30 m/s, so that flow is always mixed for sufficiently high gas velocities. The purpose of this is to deal with edge cases such as very high void fractions where the predicted value of v_{crit} is very large, where the code would otherwise predict stratified flow where the data shows mixed flow.

The transitions for the various non-stratified flow regimes are derived from the transitions in the vertical pipe flow regime map. The transition from bubbly to slug flow is based upon work by Taitel, Bornea, and Dukler:

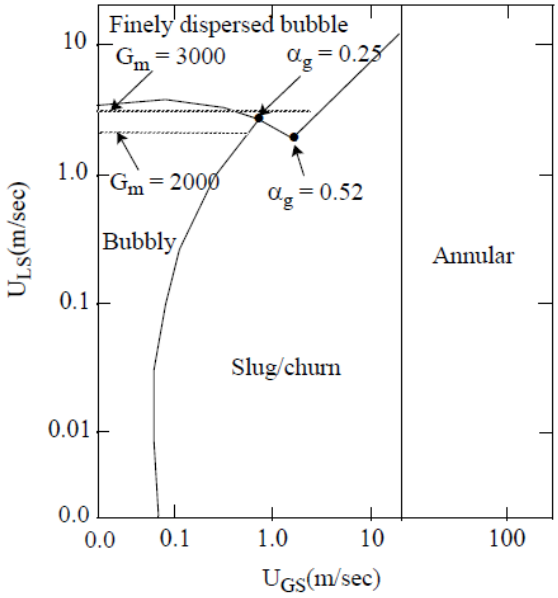

Figure 3 TBD flow regime map (air/water, 25°C, 100 kPa, 5.0 cm vertical tube) [7]

The lower limit for α_{BS} is 0.25, around when the bubble spacing decreases to about half the bubble radius, based on bubbles coalescing at this point according to Taitel, Bornea, and Dukler. This is based upon multiple other references, with 0.25 falling into reasonable agreement with these references. The upper limit for α_{BS} is 0.5, as if the void fraction were to exceed 0.52, bubbles in a cubic lattice would be touching, thus assuming high turbulence due to high flow, this is the upper limit for bubble flow. The value of α_{BS} is linearly interpolated from its lower limit of 0.25 to its upper limit of 0.5 for flow rates between $2000\,\mathrm{kg/m^2s}$ and $3000\,\mathrm{kg/m^2s}$.

Transition to annular mist flow is derived from a model by Barnea which shows annular flow for $\alpha_g > 0.76$, agreeing with experiments on vertical cocurrent upflow, including air-water experiments at standard atmospheric conditions for 2.5 cm and 5.1 cm tubes. The RELAP5 code uses $\alpha_{DE} = 0.75$ and $\alpha_{SA} = 0.80$ for the transition. To ensure a smooth transition from annular mist flow to single-phase vapour flow, a transition to dispersed flow is used at a void fraction $\alpha_{AM} = 0.9999$ [7].

4.2.2 The Vertical Flow Regime Map

RELAP5 uses a three-dimensional flow regime map for vertical flow. The three variables are a volume flux (mass flux G divided by average mixture density; essentially a weighted average flow speed), void fraction, and the wall-to-fluid temperature difference. The latter permits the inclusion of additional flow regimes corresponding to transitional and film boiling at the walls, which RELAP5 considers when dealing with vertical flow. The post-dryout regimes considered

are inverted annular (liquid core containing bubbles, surrounded by a vapour annulus), inverted slug (liquid slugs within a vapour flow), and post-dryout mist flow. The pre-CHF flow regime map is constructed in a similar manner to the flow regime map for horizontal flow [7].

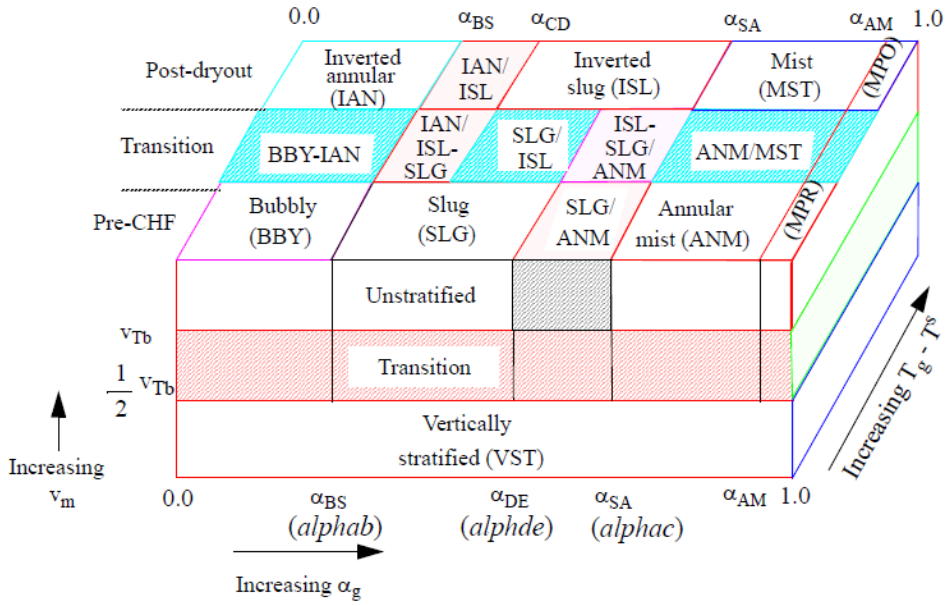

Figure 4 Flow regime map plot for vertical pipes in RELAP5 [7]

Vertically separated flow occurs when the flow is slow enough that an interface between liquid and vapour may form. The primary requirement is that the mixture velocity v_m is less than the Taylor bubble rise velocity v_{Tb} [7]:

$$v_{Tb} = 0.35\sqrt{\frac{gD(\rho_f - \rho_g)}{\rho_f}} \tag{2}$$

The second criterion ensures that vertically stratified flow only appears where it logically makes sense. RELAP5 determines, for each node, the “above volume” with the lowest void fraction and the “below volume” with the highest void fraction. The “above volume” must have a void fraction of at least 0.7, and at least 0.2 more than for the node under consideration. The node under consideration must also have a void fraction of at least 0.2 more than the “below volume”. Such a case may arise during stagnant conditions in a vertical channel where the node under consideration contains the liquid vapour interface. In addition, to ensure that only a single volume in a stack may be vertically stratified, the *liquid* fraction of the volume must be greater than the void fraction of the “below volume”, but less than the void fraction of the “above volume” (the “above volume” is ignored if it is a dead-end). Finally, the void fraction of the node must be between 0.001% and 99.999%, so that a flow that is very nearly single-phase is not treated as vertically stratified.

The transition from bubbly flow to slug flow is derived from Taitel, Bornea, and Dukler, similarly to horizontal flow. However, for vertical flow, the rise velocity of small bubbles, i.e.

$$v_{sb} = 1.53\left(\frac{g(\rho_f - \rho_g)\sigma}{\rho_f^2}\right)^{\frac{1}{4}} \tag{3}$$

must be less than the rise velocity of the Taylor bubbles, otherwise bubbles will coalesce and preclude bubbly flow. The velocities become equal for a pipe diameter of: [7]

$$D_{crit} = 19.11\sqrt{\frac{\sigma}{g(\rho_f - \rho_g)}} \tag{4}$$

In RELAP5, the coefficient 19.11 is replaced with 22.22 for better agreement with data, and then used in the void fraction criterion for slug flow [7]:

$$\alpha_{BS} = \begin{cases} \alpha_{BS}^* & G_m \leq 2000 \\ \alpha_{BS}^* + \dfrac{0.5 - \alpha_{BS}^*}{1000}(G_m - 2000) & 2000 < G_m < 3000 \\ 0.5 & G_m \geq 3000 \end{cases} \tag{5}$$

$$\alpha_{BS}^* = \max\left(0.25\min(1, (0.045D^*)^8),\ 10^{-3}\right), D^* = D\sqrt{\frac{g(\rho_f - \rho_g)}{\sigma}} \tag{6}$$

If the pipe diameter is sufficiently large so that small bubbles rise more slowly than Taylor bubbles, then α_{BS}^* is equal to 0.25 and the condition is identical to that for horizontal pipes. If the pipe diameter is smaller, then the threshold decreases rapidly (8th power of the diameter) down to a minimum of 0.001 for slug flow.

Transition from slug flow to annular mist flow is significantly more complex. It is based upon the transition from churn flow to annular flow from not only Taitel, Bornea, and Dukler, but also Mishima and Ishii. Two criteria are established. The first criterion is a transition due to flow reversal in smaller tubes, while the second criterion is a transition due to entrainment in larger tubes. The critical values for these criteria were calculated by McQuillan and Whalley, for a diameter range of 1.0 cm to 10.5 cm over many different fluid conditions. From Putney, annular flow occurs when *either* criterion is met, with the controlling criterion thus depending on the pipe diameter. RELAP5 applies these criterion to larger tubes and rod bundles in absence of any reason not to.

The criterion can be expressed in terms of void fraction to fit within RELAP5's flow regime map. The flow reversal criterion, for upflow, is [7]:

$$\alpha_{crit}^f = \frac{1}{v_g}\sqrt{\frac{gD(\rho_f - \rho_g)}{\rho_g}} \tag{7}$$

For downward flow and countercurrent flow, the flow reversal mechanism breaks down and the simpler criterion $\alpha_{crit}^f = 0.75$ is used [7]. The entrainment criterion is:

$$\alpha_{crit}^{e} = \frac{3.2}{v_g}\left(\frac{g\sigma\left(\rho_f - \rho_g\right)}{\rho_g^2}\right)^{\frac{1}{4}} \tag{8}$$

The transition to annular flow, α_{SA}, will use the lower of α_{crit}^{f} and α_{crit}^{e}. However, it must always fall in the range of:

$$\alpha_{AM}^{min} = 0.5 \leq \alpha_{SA} \leq \alpha_{BS}^{max} = 0.9 \tag{9}$$

Such conditions may be violated for very high or very low vapour velocities. The minimum void fraction α_{AM}^{min} where annular flow can possibly exist is 0.5, while the maximum void fraction α_{BS}^{max} where slug flow can possibly exist is 0.9. If the transition criteria predict a threshold outside this range, then α_{SA} is clamped within this range.

Transition to dispersed flow is the same as horizontal pipes ($\alpha_{AM} = 0.9999$). The remaining void fraction thresholds are offset from α_{BS} and α_{SA}:

$$\alpha_{CD} = \alpha_{BS} + 0.2 \tag{10}$$

$$\alpha_{DE} = \max(\alpha_{BS}, \alpha_{SA} - 0.05) \tag{11}$$

From De Jarlais and Ishii, the post-dryout flow regime transition criteria match with their respective pre-CHF flow regime transitions. Bubbly flow becomes inverted annular, slug flow becomes inverted slug, and annular-mist flow becomes mist/droplet flow. A transitional region exists as it appeared to be appropriate.

On a final note, a theory by Kocamustafaogullari, Chen, and Ishii precludes slug flow for very large pipes, and some experimental evidence supports this. In the code, the threshold is 8 cm, above which the code will use bubbly and churn-turbulent correlations rather than slug flow correlations.

4.3 Heat Transfer Correlations in RELAP5

RELAP5/MOD3.3 has a large number of wall heat transfer correlations, and defines 12 possible heat transfer modes, e.g. nucleate boiling, transition boiling, and film boiling. The code allows user to specify the types of flow field (or hydraulic geometry). It uses the built-in logic to select the appropriate heat transfer modes and heat transfer correlations for a specified geometry [7]. The default geometry, i.e. type-101, is used for most applications, and all the other types modify some of the standard correlations within type-101.

Type-101 uses the Chen correlation [8] for both saturated and subcooled nucleate boiling. The subcooled liquid condition was taken into account by using the bulk liquid temperature as reference temperature for the convective part [7]. Chen's transition boiling model [9] was used for transition boiling. For film boiling, three heat transfer mechanisms are considered including conduction across a vapor film blanket next to a heated wall, convection to the flowing vapor and between the vapor and droplets, and radiation across the film to a continuous liquid blanket or dispersed mixture of liquid droplets and vapor [7]. The Bromley correlation [10] was used as a model basis for conduction, the Dittus-Boelter with gas properties for convection, and Sun

correlation [11] for radiation. The 1986 AECL CHF Lookup Table by Groeneveld et al. [12] was used to predict CHF and multiplying factors are applied for geometry specific corrections.

Table 1 Relevant Wall Heat Transfer Correlations in RELAP5/MOD3.3 [7]

	Modes of Heat Transfer							
Geometry Type	Lamin-ar	Natural	Turbulent	Conden-sation.	Nucleate Boiling	Transition Boiling	Film Boiling	CHF
101 (default)	Sellars Nu = 4.36	C-Chu or McAdams	Dittus-Boelter	Nusselt Chato-Shah-Coburn-Hougen	Chen	Chen	Bromley	Table
124 (CANDU)	Nu = 4.36	C-Chu or McAdams	Dittus-Boelter	Nusselt Chato-Shah-Coburn-Hougen	Chen	Chen	Bromley	Table

5. RELAP5 Code Architecture

5.1 Flow Regimes

The determination of flow regime for each volume at each point in time during the simulation allows for the appropriate application of the constitutive relations used for interphase drag and shear, wall friction, wall heat transfer and interphase heat and mass transfer. These parameters are important for the accurate prediction of the physical behaviour associated with IBIF conditions, and as such, the application of appropriate flow regimes is under investigation in this study. As described above RELAP5 has four options for the decision logic used to determine flow regime that depend only on the type of hydraulic component: horizontal volume, vertical volume, high-mixing volume and ECC mixer volume. For this study, the heated channel of the CWIT facility is modeled by a horizontal hydraulic component and as such, only the horizontal flow regime map is discussed.

Figure 5 shows the overall logic for the subroutine $horizhifreg$ in which the flow regime is determined for a horizontal volume. This subroutine is called only once in the entire code from $phantv$ (a subroutine that determines the constitutive parameters for interfacial heat transfer and shear stress). Immediately prior to the call to $horizhifreg$, several flow regime parameters are initialized ($fstrat$, $fbub$, $fslug$, $fanm$, and $fdis$). Each of these can have a value between 0.0 and 1.0 and are used in subsequent subroutines to ensure smooth transitions between the correlations used in determining the aforementioned constitutive parameters.

The first step in $horizhifreg$ is a calculation of the collapsed liquid level within the volume that is based entirely on the void fraction. A critical stratification velocity $vcritl$[1] is then determined using the void fraction, phasic densities and the user-input geometry of the volume and is

[1] A more detailed discussion of $vcritl$ findings can be found below.

compared with the relative velocity of the gas and liquid phases ($rvcrit = |velg - velf|/vcritl$). If $rvcrit \geq 1.0$, the flow is considered to be fully mixed and the parameter $fstrat$ (which is a measure of flow stratification) maintains a value of 0.0. If $rvcrit < 1.0$, the extent of stratification, $fstrat$, is calculated based on $rvcrit$, void and the average mixture mass flux. Several limits are then placed on $fstrat$ based on previously reported code errors. Some combinations of physical parameters that do not correspond to stratified conditions were found to produce stratification within the code. As such, $fstrat$ is ramped to 0.0 between superficial gas velocities of $10 - 30\ m/s$ for non-CANDU geometries and between superficial liquid velocities of $0.085 - 10\ m/s$ for CANDU geometries.

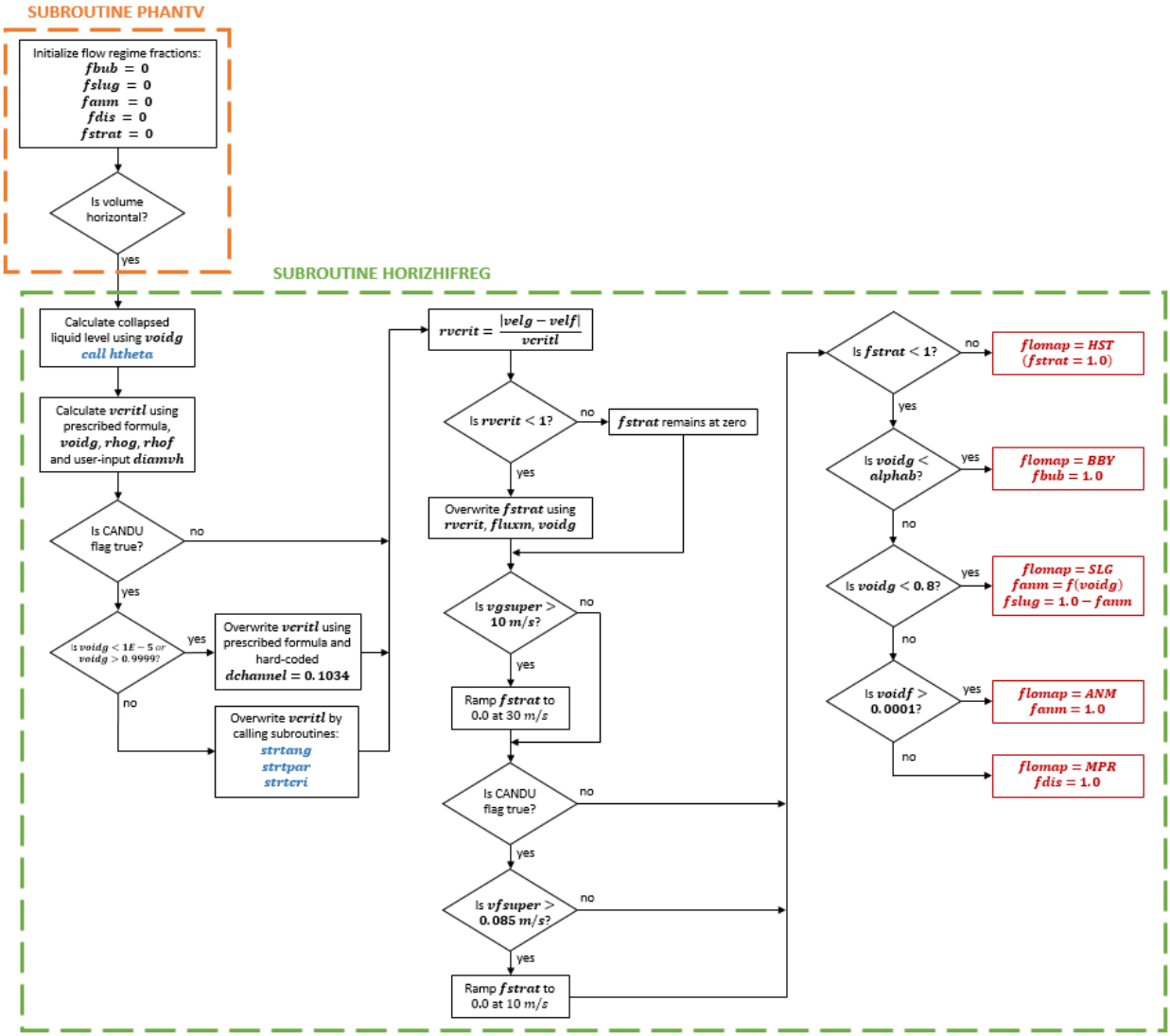

Figure 5 Flow chart of the flow regime decision logic implemented in the RELAP5 source code

The simulation of the low-flow and low-power conditions associated with IBIF rests heavily in the ability of the code to predict stagnant and stratified behaviour in a horizontal fuel channel. These conditions fall under the category of HST flow regime, and so the transition between HST flow and normal, higher-flow regimes is very significant to this study. The v_{crit} parameter described by Eq (1) represents the limiting relative velocity of the gas and liquid phases above which

instability between the two phases will occur and give rise to intermittent flow. Below this relative velocity, the phases are assumed to be stratified. It was found that within the source code, Eq (1) is simplified in the following way:: It

Manual: $$v_{crit} = \frac{1}{2}\left[\frac{(\rho_f - \rho_g) g \alpha_g}{\rho_g sin\theta} \cdot \frac{A}{D}\right]^{1/2} (1 - cos\theta) \quad (12)$$

Source Code: $$v_{crit} = \frac{1}{2}\left[\frac{(\rho_f - \rho_g) g \alpha_g}{\rho_g sin\theta} \cdot \frac{\pi D}{4}\right]^{1/2} (1 - cos\theta) \quad (13)$$

This simplification is only true when the hydraulic diameter of the volume is equal to the geometric diameter (ie. a simple circular pipe with no internal geometry present). The geometric and hydraulic diameter associated with the CANDU bundle geometry are 10.34 cm and ~ 0.7 cm respectively. This is a significant discrepancy that should be addressed in future releases of RELAP5.

It has also been noted that the documented stratification condition of $1/2\ v_{crit}$ and $2500\ kg/m^2 s$ shown in Figure 1 is not what is found in the code (v_{crit} and $2500\ kg/m^2 s$). When the CANCHAN component is used, $vcritl$ is calculated in a different way. If the void fraction is either very high (0.9999) or very low (0.0001), $vcritl$ is calculated using Eq (13) with one modification: the diameter is hard-coded to be $dchannel = 0.1034\ m$ for a typical inner diameter of a CANDU pressure tube. This is important information for the RELAP user to be aware of. It means that the CANCHAN functionality of tracking the collapsed liquid level and implementing different heat transfer coefficients to covered and uncovered elements is currently only applicable to an uncrept and hard-coded value. If the void fraction is not beyond these limits, the following three subroutines are called in succession in order to calculate $vcritl$[2].

- $strtang$: get subtended angle in stratified flow
- $strtpar$: calculation of the effective length scale for hydrostatic interphase pressure difference in circular channels with or without pins as well as rectangular channels plus their derivatives w.r.t. void fraction
- $strtcri$: obtain stratification criteria based on relative phase velocity and prescribed CANDU-specific relations

Within $strtang$, the liquid level is obtained using the void fraction and $dchannel$ (hard-coded). With a bundle cross-sectional geometry, the relationship between void and liquid level cannot be determined analytically, so it is calculated iteratively. The function does not use any information about the input file heat structures (these are over-ridden by hard codded values for 37 element fuel), and so again it is important for the user to be aware that the results of this subroutine are valid for only a prescribed 37-element geometry.

5.2 Heat Transfer Regimes

Figure 6 shows the flow diagram documented in the RELAP5 theory manuals describing the logic used in determining the heat transfer regime for wall-to-fluid heat transfer. After careful

[2] The initial descriptions in this list are taken verbatim from the comment section in each subroutine and will be described in more detail.

examination and comparison with the source code, it has been found that the documented logic is consistent with the coded logic. The majority of these conditional statements are implemented in the subroutine $htrc1$. This subroutine is called from $htcond$ which returns the left and right boundary conditions for a heat structure. Within the $htrc1$ architecture, conditional statements based on the fluid and heat structure conditions (T_{fluid}, T_{sat}, T_{wall} and α) are followed until a heat transfer regime has been determined. Once the regime has been determined, the appropriate subroutine is called to calculate the heat transfer coefficient.

The subroutines containing the heat transfer correlations are:

- $conden$: when the wall temperature is below the saturation temperature of the fluid
- $dittus$: single-phase liquid or vapor conditions
- $chfcal$: calculates the CHF (default is the 1986 LUT method)
- $prednb$: nucleate boiling for all surfaces except horizontal bundles
- $prebun$: nucleate boiling for horizontal bundles
- $suboil$: vapor generation rate in superheated liquid next to the wall when the bulk liquid is subcooled
- $pstdnb$: transition and film boiling

For reference, Table 2 shows the numbering convention for all possible modes of heat transfer within the RELAP5 coding architecture. The most significantly observed regimes in the simulations presented in this report are highlighted.

Table 2 Modes of Heat Transfer in RELAP5 Source Code

Code Label	**Mode of Heat Transfer**
0	Convection to noncondensable-steam-water mixture or superheated liquid
1	Convection at supercritical pressure or superheated wall with negative heat flux due to superheated gas
2	Single-phase liquid convection at subcritical pressure, subcooled wall and low void fraction
3	Subcooled nucleate boiling
4	Saturated nucleate boiling
5	Subcooled transition boiling
6	Saturated transition boiling
7	Subcooled film boiling
8	Saturated film boiling
9	Single-phase vapor or supercritical two-phase convection
10	Condensation when void is less than one
11	Condensation when void is one
12	Single-phase liquid convection at subcritical pressure, subcooled wall and low void fraction, uses alternative correlations

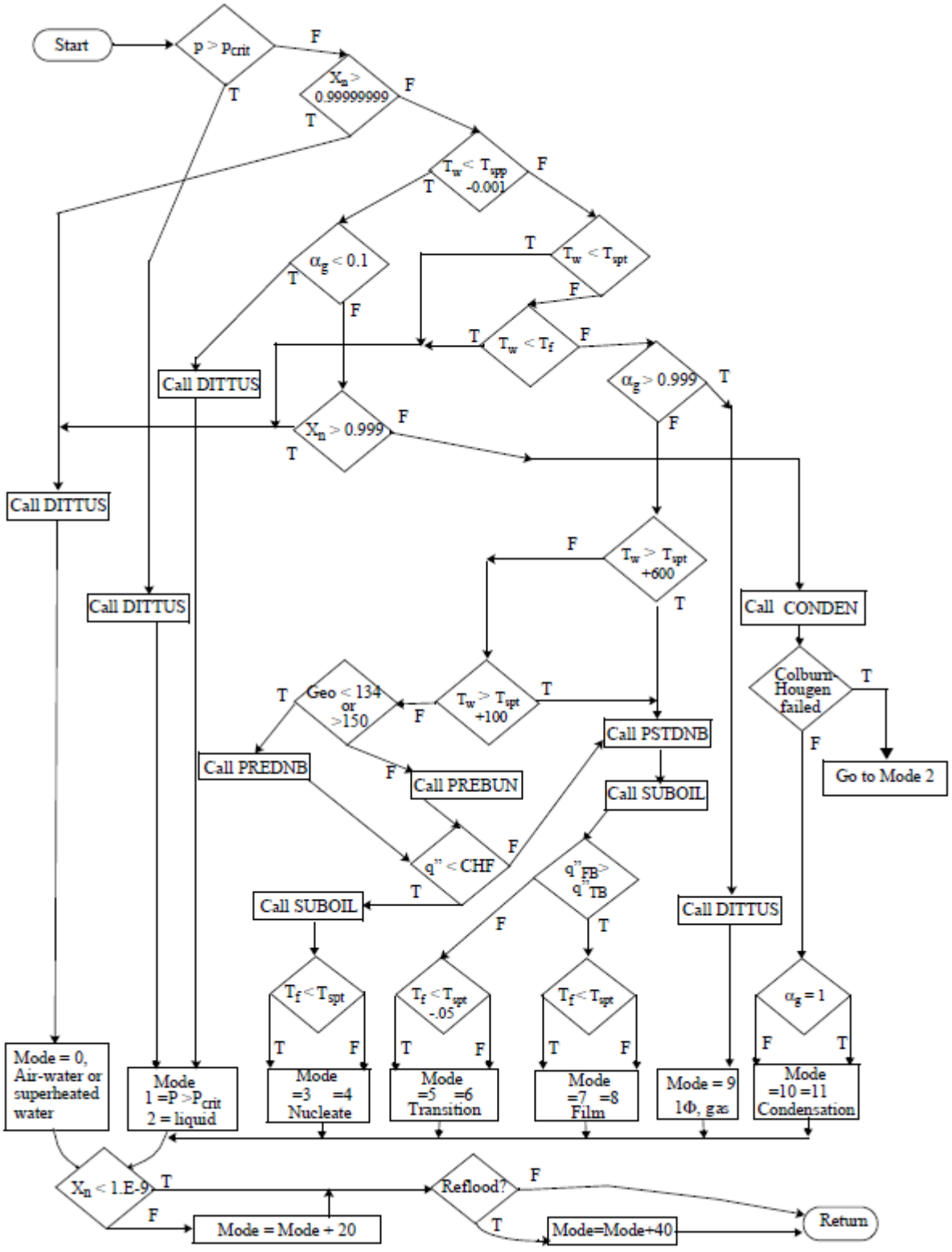

Figure 6 RELAP5 logic for wall-to-fluid heat transfer regimes [7]

In some cases, the code further categorizes the applied correlations based on a user-specified geometry parameter. In a RELAP simulation input file, the user must specify a heat structure

geometry type from a prescribed list. Within each of the subroutines listed above, conditional statements based on this geometry type are implemented in order to apply the correct correlation. There are three geometry types that are of immediate interest to this study: 101 (the default geometry which is a single, vertical rod), 134 (the standard horizontal bundle) and 124 (the CANDU bundle). It stated that [7]:

1) Type 134 uses all of the same correlations as type 101 except in nucleate boiling and CHF
2) Type 124 uses all of the same correlations as type 101 with one modification: if the flow regime is stratified, the void fraction is temporarily altered based on the height of the heat structure

The $dittus$ subroutine is called when either single-phase vapour or liquid convection is occurring. This routine calculates the Nusselt number for laminar flow, turbulent flow and natural convection and uses the maximum of the three resulting numbers. For laminar flow, all three geometry types use the same formula developed by Sellars, Tribus and Klein [13]:

$$Nu = 4.36 \tag{14}$$

For turbulent flow, the Dittus-Boelter correlation is used [14] [15]:

$$Nu = 0.023 Re^{0.8} Pr^{0.4} \tag{15}$$

With the exponent on the Prandtl number hard-coded to be 0.4 for all cases. However, it is of note that within the code, when the boundary condition type 134 is used, Eq (15) is modified to account for cross-flow within the bundle. This modification is not implemented when the CANDU bundle condition is used.

For natural convection, the McAdams correlation for a flat plate with energy flowing vertically is used [15]:

$$Nu_L = 0.27 Ra_L^{0.25} \tag{16}$$

Similar to the turbulent flow term, a modification is made within the code to account for cross flow within the bundle (again such enhancements are not included in the CANDU bundle features).

In both the turbulent forced flow and natural convection cases, the cross-flow correction term depends on the geometry of the bundle. The user has the ability to apply a pitch-to-diameter ratio on the additional boundary condition cards and this value must be carefully chosen. For PWR fuel assemblies with a square lattice, the pitch-to-diameter ratio is well-defined parameter. For the circular CANDU bundle, it is not. Additionally, if the user selects the CANCHAN component and type 124 convective boundary condition, this pitch-to-diameter parameter has been designated to be the height of the fuel element within the channel. Careful consideration must therefore be given when making these choices in the input deck. Such routines also may require modification to account for lateral “frothy” behavior wherein some liquid is transported from the lower liquid elevations in a channel to the steam bubble.

In should also be noted that the $prebun$ subroutine uses different correlations for nucleate boiling than the $prednb$ subroutine due to the different geometry of heat transfer surfaces. This is currently implemented clearly for a 134 boundary condition, but not when the 124 boundary condition is used. This discrepancy should be addressed in future releases of RELAP5 since the CANDU bundle geometry should receive the same treatment.

Regarding the CANCHAN component and type 124 combination, it is important for the user to be aware of the limits placed on the parameters entered on the heat structure cards. The following rules must be followed:

Table 3 Rules for use of CANCHAN Component

Parameter	**Rule**
Natural convection length	Must be the inner diameter of the pressure tube
Heated equivalent diameter	Must be the outer diameter of a fuel rod
Number of heat structures	Must be 37

If any of the rules listed in Table 3 are not adhered to, the channel will not be represented correctly. Additionally, the only modification made in the determination of heat transfer coefficients occurs in the subroutine $htrc1$. If these conditions are met the following process occurs:

1) The current void fraction ($voidg$) is stored in a temporary variable $voidg\_temp$
2) The collapsed liquid level is calculated ($hzmix$)
3) Using $pitdia$ (the height of the current heat structure), $htdiam$ (heated equivalent diameter), and the natural circulation length, the liquid level is determined to be either:
   - Above the heat structure (and $voidg$ is temporarily set to 0.0)
   - Below the heat structure (and $voidg$ is temporarily set to 1.0)
   - Between the top and bottom of the heat structure ($voidg$ is set between 0 and 1)
4) The subroutine then proceeds normally to calculate the heat transfer coefficient for the surface and concludes with the reassignment of the original void fraction to the variable $voidg$.

One final comment can be made regarding the CANCHAN component. It has been found that when CHF is determined at each time step for each heat structure, if the geometry type has been specified as 124, the code calls $chfd2o$ instead of $chfh2o$, regardless of the fluid type specified within the system. This may cause inaccuracies within the simulation and should be addressed in future releases of the code.

6. The Cold Water Injection Test Facility

In March, 2001, Ontario Power Generation contracted and funded a series of standing-start tests at the CWIT Facility located at Stern Laboratories in Hamilton, Ontario. This test program was specifically designed to provide experimental data to be used for the development and validation of computer codes for the nuclear industry [16]. For this study in particular, data from the standing-start tests can be used to ascertain the accuracy of predictions of fuel element and pressure tube surface temperatures, liquid level determination within the channel, and void fraction in the feeders (ie. venting).

6.1 Facility Description

The system used for the standing-start test series is referred to as a double break (i.e., both inlet and outlet headers are open to the atmosphere), double injection configuration and is shown in a simplified schematic in Figure 7. The test loop consists of one electrically heated flow channel assembly of the same geometry as a CANDU pressure tube (including full-scale

CANDU 6 end-fittings). The channel is connected by feeder pipes to an inlet and outlet header located $10\ \mathrm{m}$ above the channel. The remaining components of the test loop consist of the balance of plant: injection lines, break lines, a blowdown tank, pumps, pressure and temperature control systems and all interconnecting piping [16].

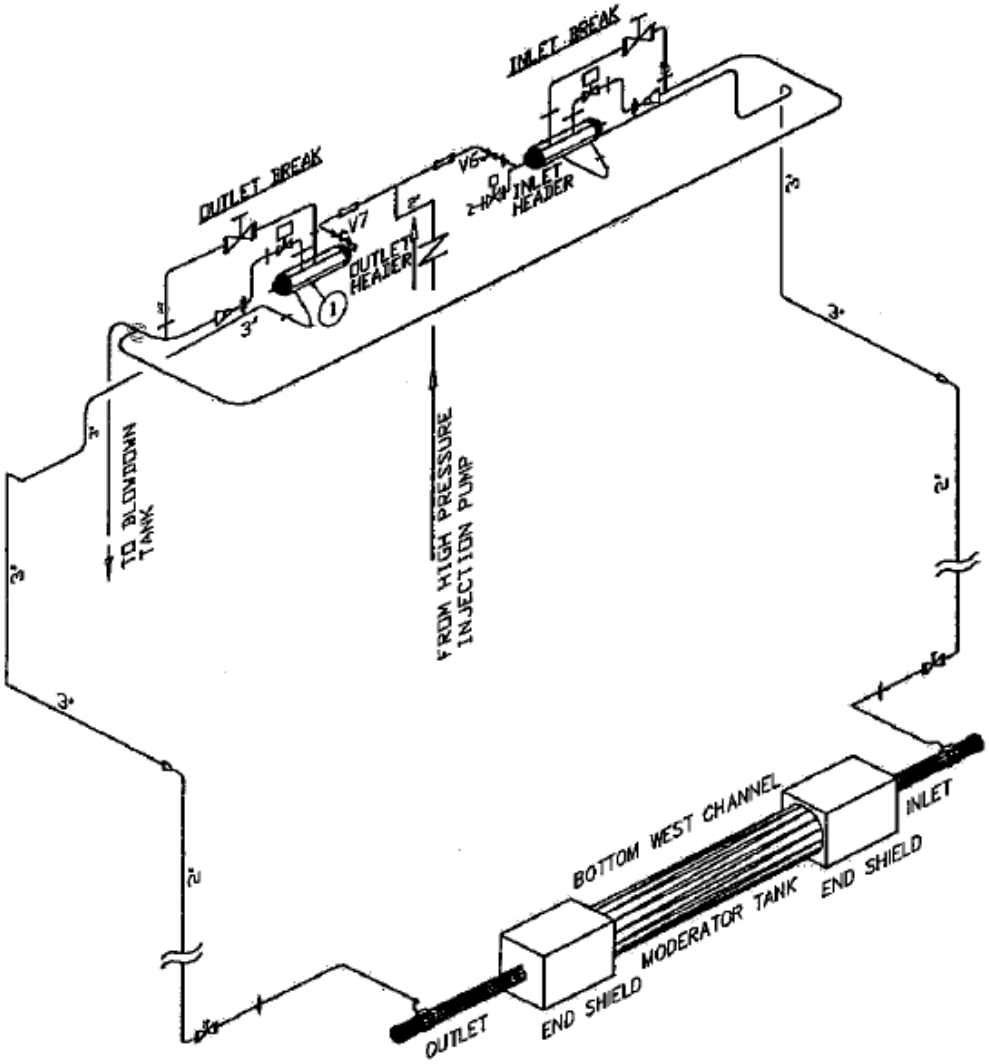

Figure 7 Schematic of the CWIT facility [16]

The facility was designed to be capable of of the following test conditions:

- System pressures of $0.11 - 7.0\ \mathrm{MPa}$
- Initial system temperatures of $30 - 178℃$
- Total injection water flow rates of $0 - 5\ \mathrm{kg/s}$
- Total channel powers of $7 - 200\ \mathrm{kW}$

6.1.1 Headers

Each of the headers are made of 10” SCH 120 carbon steel pipe with several flanged connections as shown in Figure 8. For the standing-start tests, the connections shown in grey in Figure 8 were blanked. The inlet and outlet injection lines connect to the corresponding header parallel to its axis and at a vertical height of 3” below the centreline.

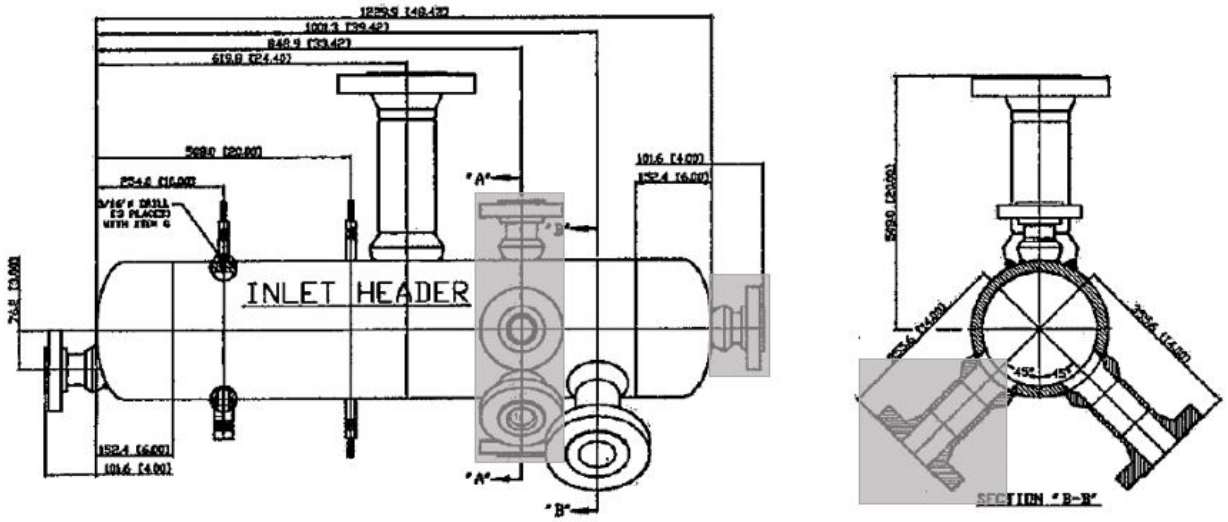

Figure 8 Engineering drawings of the CWIT facility headers

6.1.2 Injection and Blowdown Lines

The water injection system consists of four pumps capable of imposing total inlet injection flow rates in the range of $0 - 5\ \mathrm{kg/s}$. Each of the lines leading to the inlet and outlet headers are equipped with a venturi meter, an isolation valve and a K-factor orifice for controlling the symmetry of injection. The entirety of the injection system utilized in this test series is comprised of carbon steel, 2” SCH 80 piping [16].

The blowdown lines in use for this test series are comprised of 4” SCH 40 carbon steel lines coming vertically off of each of the headers (as seen in Figure 8). Each line is equipped with a fast-acting blowdown valve used to allow control of the timing and symmetry of the simulated breaks. The lines are then widened to 8” SCH 40 piping, joined, directed to a blowdown tank and then recirculated to be cooled/heated and re-injected through the total injection line.

6.1.3 Feeder Pipes

The inlet and outlet feeders are comprised of 2” SCH 80 (connecting to the end-fittings) and 3” SCH 80 (connecting to the headers) carbon steel piping. The general geometry can be clearly seen in Figure 7 with the following notable comments. The 3” lines connect to the headers at an angle of $45°$ below the horizontal and the 2” lines connect to the end-fittings at an angle of $32°$ below the horizontal [16]. The feeders are wrapped in $50\ \mathrm{mm}$ thick high temperature fibreglass insulation to prevent significant heat loss to the atmosphere [6].

6.1.4 Channel and End-Fittings

The test channel itself was constructed to simulate a single full-scale CANDU fuel channel. It includes 37 electrically heated fuel element simulators (FES) assembled in the CANDU-6 fuel bundle geometry. The FESs and pressure and calandria tube are instrumented with 100 internal and 36 external thermocouples at 16 radial and 8 axial positions along the heated length of the channel. The channel also includes full-size stainless steel CANDU-6 end-fittings with modifications made to accommodate the extensions of the FES required for the application of electrical power to the channel.

Figure 9 illustrates the geometry of the channel and end-fittings. The top figure shows an engineering drawing of the end-fittings used in the CWIT facility. The most significant difference between the CWIT facility setup and the operational CANDU setup is the presence of baffle plates used to secure the unheated FES extensions. It is reported that these baffle plates provide a near water-tight seal, and as such, flow to the dead space in the centre of the end-fittings is assumed to be zero [6]. The bottom three figures illustrate the regions of flow (highlighted in light blue) for each significant geometrical section in the channel-end-fitting configuration.

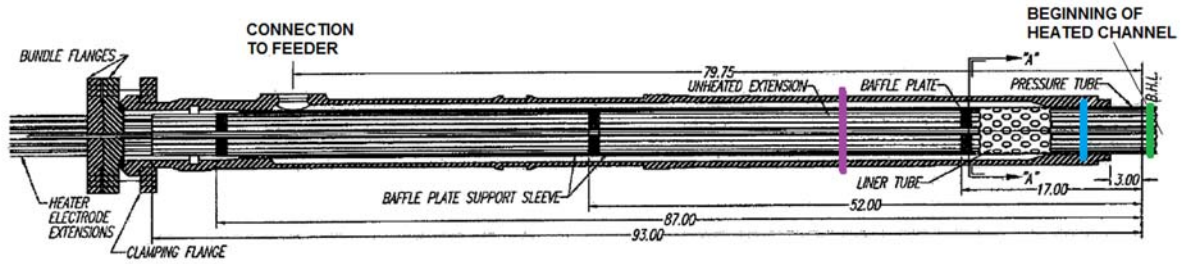

Figure 9 Engineering drawing of the CWIT facility end-fitting

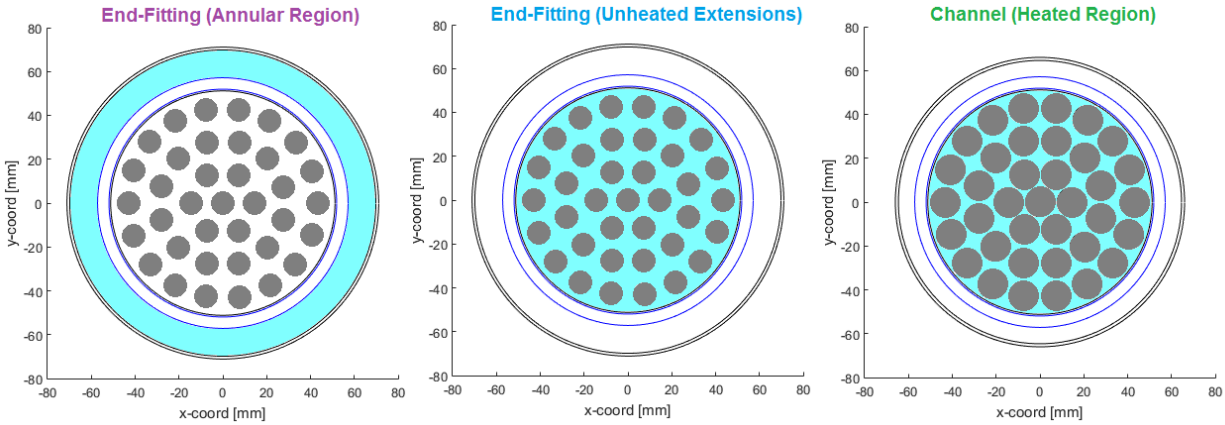

Figure 10 Cross-sectional views of relevant end-fitting locations corresponding to Figure 9

Each FES consists of an insulated support (slug) in the centre surrounded by a filament made of Inconel-600 and inner alumina sheath to electrically isolate the filament from the outer sheath.

The outer sheath is constructed from Inconel-600 and has the outer diameter of a typical CANDU fuel sheath ($13.08\ \mathrm{mm}$). The inner and outer diameters of the pressure tube (made of Zr-Nb) are $103.886\ \mathrm{mm}$ and $114.3\ \mathrm{mm}$ respectively. Along the heated portion of the channel, the inner and outer diameters of the calandria tube (made of Zr) are $129.2\ \mathrm{mm}$ and $131.994\ \mathrm{mm}$ respectively. In the annular flow portion of the end-fitting, the calandria tube is wider with inner and outer diameters of $139.7\ \mathrm{mm}$ and $142.24\ \mathrm{mm}$ respectively. The unheated extensions of the FES strings have an outer diameter of $9.53\ \mathrm{mm}$.

Within the channel, the heated length of the FES assembly is reported to be $6.099\ \mathrm{m}$. The axial power distribution is a smooth cosine shape with a maximum peak at the centre of the channel of 1.485 times the average power of the assembly and minimum values at the ends of 0.15 times the average power. The ratio of heat generation per pin in each ring of pins (from the outer ring to the central pin) is $1.0/0.81/0.72/0.68$.

6.2 RELAP5 Model of Facility

Figure 11 shows a simplified breakdown of the modules of the experimental facility and the numbering convention used within the RELAP5 realization of the facility.

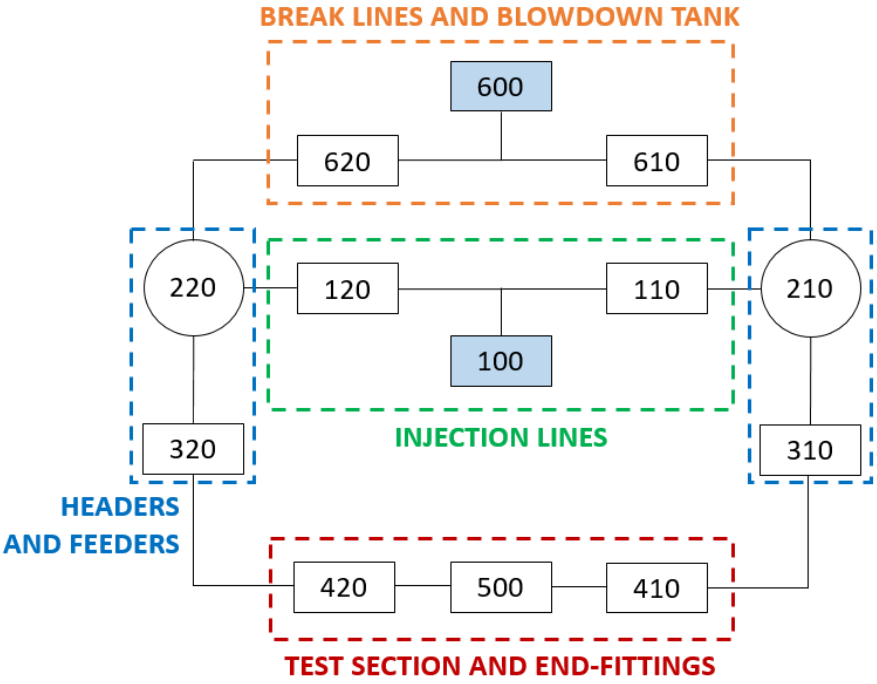

Figure 11 Numbering convention for RELAP5 model of CWIT facility

6.2.1 Injection and Blowdown Lines

The common injection line is instrumented with a pressure and fluid temperature measurement approximately 1.5 m below the header centerline. For this reason, the time-dependent volume

that models the inlet conditions (component 100) has been placed here. Similarly, a pressure measurement located at the junction between the two break lines dictated the location of the outlet time-dependent volume (component 600).

With the realization that a full dataset for the experiments would not become available, several changes were made in order to reduce simulation time. A large portion of the injection and break lines included in the original input decks were removed. These lines were originally included with the intent of using the indicated pressure and temperature measurement sites as accurate boundary conditions during the transient. Due to the low (zero) flow conditions of these experiments, the change in location of the initial boundary condition dictating temperature and flow rate was found to cause no detectable change in the results of the simulations. Similarly, when a portion of the break lines was removed, the outlet pressure boundary condition applied here yielded no change in the reported values of pressure (in the inlet header) and saturation temperature (in the channel).

6.2.2 Headers

Figure 12 shows a diagram of the inlet header and its reference nodalization scheme. The total length of the header has been divided into 5 volumes of equal, and is represented by a pipe component with a horizontal orientation. At each of the junctions to the connecting pipework, the offtake model is applied in order to allow for the possibility of single-phase flow during stratified conditions. It is of note that the location of the break line along the axis of the inlet and outlet header is different (as seen in Figure 12).

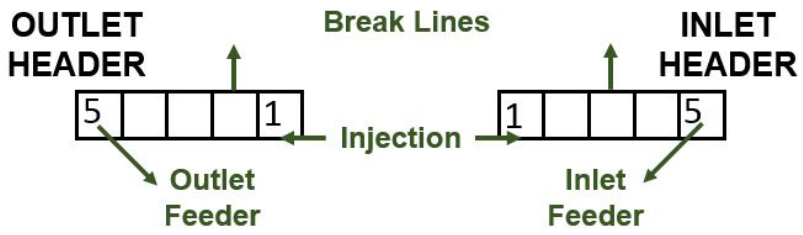

Figure 12 RELAP5 nodalization of the headers

6.2.3 Feeders

A vertical slicing methodology was applied during the nodalization of the facility. All volumes passing through a plane in vertical space have the same elevation change (specifically, the same starting and ending coordinate in the z-direction). This technique has been shown to be particularly important during simulations of natural circulation of PWRs. With low-flow conditions, the system is much more sensitive to small perturbations, and this slicing technique ensures that the changes imposed are propagated correctly.

6.2.4 Channel and End-Fittings

Figure 13 shows the current nodalization scheme for the end-fitting at the inlet side of the test section. The structures used in the facility are full-scale CANDU-6 end-fittings with only minor changes made to accommodate the facility specific details. The most notable change is the geometry that occupies the center of the fitting. The fuel element simulators are electrically heated, requiring extensions to protrude out of both ends of the channel. These unheated extensions occupy the central portion of the end-fittings in the same geometrical form as the 37-element bundle configuration of the channel. However, as stated previously, this central section of the end-fittings is significant only for its thermal properties and does not provide any volume for coolant flow.

As such, the feeder is connected to the annular flow portion of the end fitting. This portion is represented by a horizontal pipe component with 8 volumes (with the flow area and hydraulic diameter carefully calculated from the available engineering drawings). Adjacent to the annular section is a branch component representing the volume where the flow transitions from the channel geometry flow area to the annular geometry. The flow area of the volume of the branch was assigned to be that of the 37-element channel geometry with the unheated extensions (as seen in the middle of Figure 10, with a smaller element radius than the heated portion). The flow area of the junction connecting to the channel was directly calculated from the information in the drawings. The flow area of the junction connecting to the annular portion was not provided and so a careful estimation was made. The sensitivity of the results to this estimation is reported later in this document.

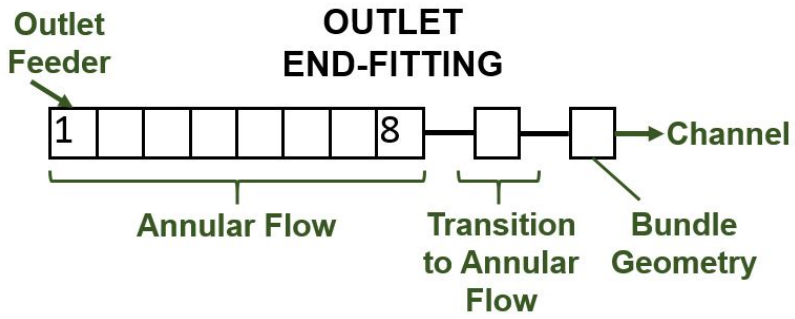

Figure 13 RELAP5 nodalization of the end-fittings

Additionally, since the condensation of vapor by the relatively cool metal within the end-fittings plays an important role in the IBIF cycle, careful attention is given to the mass of metal and the available heat transfer surface area within this component. Passive heat structures were used on each end-fitting component to represent the thermal effects of the presence of this metal. In both of the experiments under examination, no external cooling was applied to the end-fittings, and so the RELAP5 model for each reflects this.

The reference simulation for each of the experiments uses a horizontal pipe geometry for the heated section of the channel. The $6\ \mathrm{m}$ of pipe is divided into 24 volumes. The pressure tube, annulus gas and calandria tube is modelled as a heat structure connected along the entire length of the channel with the default convective boundary condition applied to the side

connected to the channel, and heat loss modelled on the opposite side of the component as given in [17][3].

37 individual active heat structures were used to simulate the FES string. For the reference simulations, these heat structures were given the standard horizontal bundle convective boundary condition with cylindrical symmetry. Figure 14 shows the material makeup and the meshpoint assignment for each heat structure. The radial power factor applied within each element was assigned to be 1.0 for the two intervals representing the heated filament and 0.0 for the remaining intervals.

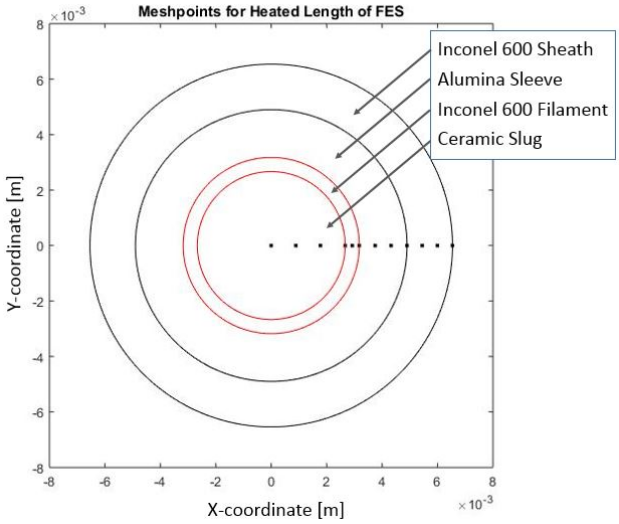

Figure 14 RELAP5 assignment of heat structure meshpoints for an individual electric fuel element simulator

Figure 15 shows the power factors applied both axially and radially within the 37-element bundle geometry. These factors were calculated based on the documented power distribution within the channel and provide a cumulative sum of 1.0. This allows for the use of one control variable with the total channel power to be applied and correctly distributed through the FES heat structures.

[3] A heat transfer coefficient of $5.9\ \mathrm{W/mK}$ was reported to be derived from measurements taken at the CWIT facility.

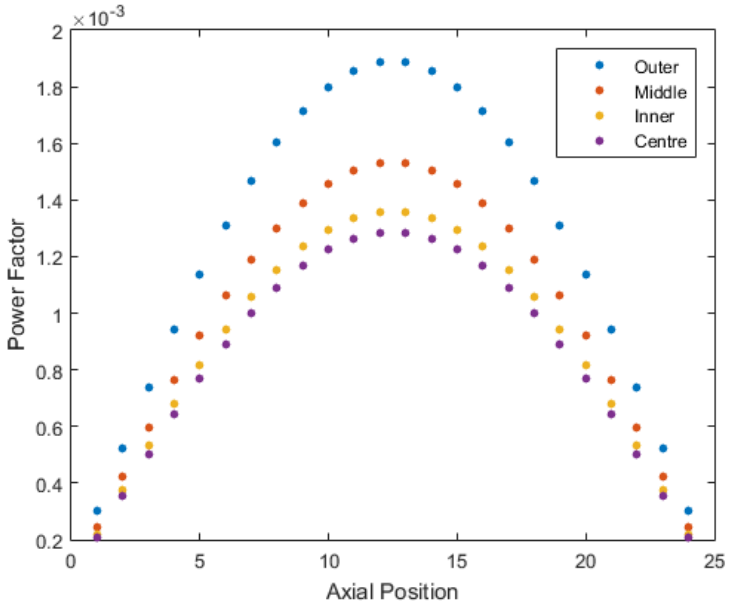

Figure 15 RELAP5 axial and radial power factors for the electrical fuel element simulators

6.3 Description of Experiments 1613 and 1617

Due to the availability of experimental data, test numbers 1613 and 1617 were chosen to be modelled. The experimental conditions are outlined in Table 4.

Table 4 Experimental Conditions for Two Standing-Start Tests [6]

Experiment	Header Pressure (kPa)	Initial Temperature (℃)	Injection Flow Rate (kg/s)	Channel Power (kW)	Saturation Temperature (℃)[4]
1613	2000	30	0	131	214.9
1617	7000	30	0	30	286.8

The following experimental procedure was followed for each of the two tests:

1) The outlet-side injection valve and inlet-side blowdown valves were closed while their counterparts were in a fully-open position. Water at the desired preheat temperature was injected into the system. With this valve configuration, flow is forced through the entire loop until the system temperature is consistently at the desired initial condition.
2) The outlet-side injection valve and inlet-side blowdown valves were then opened fully in conjunction with the inlet injection flow rate being set to the experimental condition (in these cases $0\ \mathrm{kg/s}$)
3) When the venturi meter near the channel gives a steady measurement of near-zero flow, the full channel power is switched on, indicating $t = 0$ for the resulting measured data.

[4] This measurement was reported to be taken in the channel [6]

Figure 16 shows the location within the CWIT Facility of the available temperature data. For the sake of illustration, planes B, F1 and I and pins 10 and 37 were chosen for comparison to the simulated data.

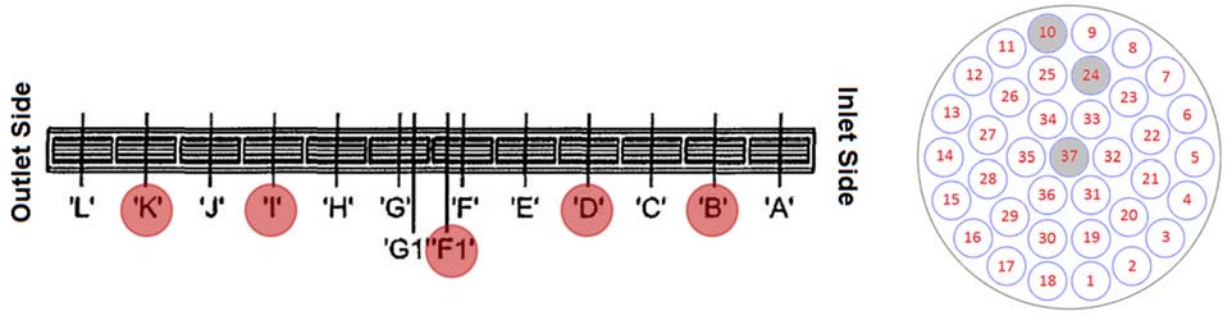

Figure 16 Locations of available CWIT facility data along the axis (left) and cross-section (right) of the heated test section

Figure 17 shows selected thermocouple channels through the entire transient of each test. All experimental data shown in this report has been digitized from a Master's thesis published in 2010 [6].

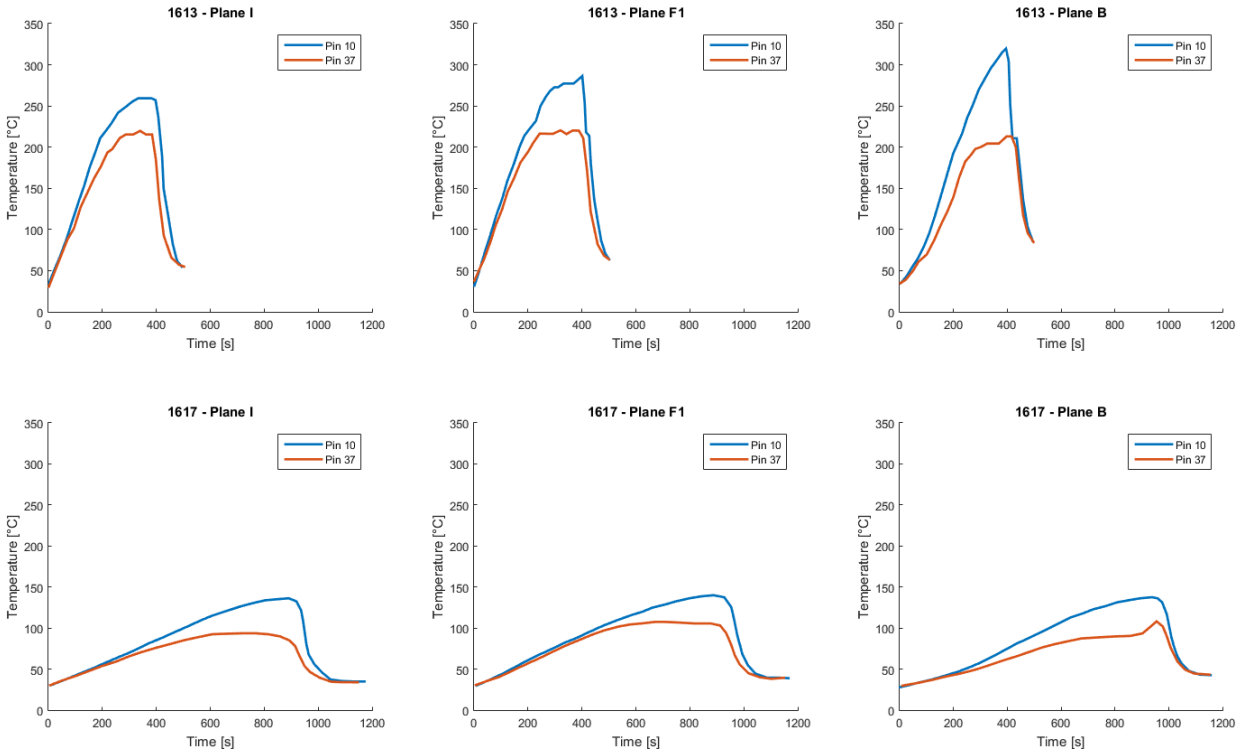

Figure 17 Selected thermocouple channels for the entire transient of tests 1613 and 1617

It can be seen that the venting time for the high-power case is approximately $400\ s$, with corresponding maximum fuel cladding temperatures of up to $319.5℃$ for pin 10 and $220.5℃$ for pin 37. For the low power case, the venting time is closer to $1000\ s$ and the maximum pin temperatures are $140.0℃$ and $108.0℃$ for pins 10 and 37 respectively.

6.4 Modelling Assumptions for the Transient

The experimental procedure outlined in the previous section was implemented using two stages of trips within the RELAP5 architecture:

1) The first trip occurs at $t = 100\ s$ and triggers the opening of the outlet-side injection and inlet-side blowdown valves (from fully closed to fully opened positions)
2) The second trip occurs at $t = 200\ s$ and triggers the onset of full power to the channel heat structures

An initial assumption was made that 100-second intervals would be sufficient time for each stage in the simulation to reach a steady state. This was subsequently confirmed by inspection of the first $200\ s$ of the simulated experiments. It was also assumed that the FES assembly reaches full power within $1\ s$ of it being turned on.

Heat loss to the environment was assumed to be negligible everywhere except in the channel. The heat loss from the end-fittings to the atmosphere was not expected to be significant [17] and initial simulations were performed with minor heat losses modeled in the feeders with no change in the global results (venting time and maximum sheath temperature).

6.5 Simulation Results

The following sections present a comparison of the available data channels for each of the two tests with the corresponding simulated data. Additional simulated parameters such as flow and heat transfer regimes are presented and discussed in Section 8. This is to allow first for the discussion of the sensitivity of the directly comparable parameters (FES sheath temperatures) to key input parameters.

6.5.1 High Power (Test 1613)

Figure 18 shows the fuel sheath temperature for the high power experiment for pins 10 and 37. Both the CWIT dataset and the RELAP5 dataset are shown.

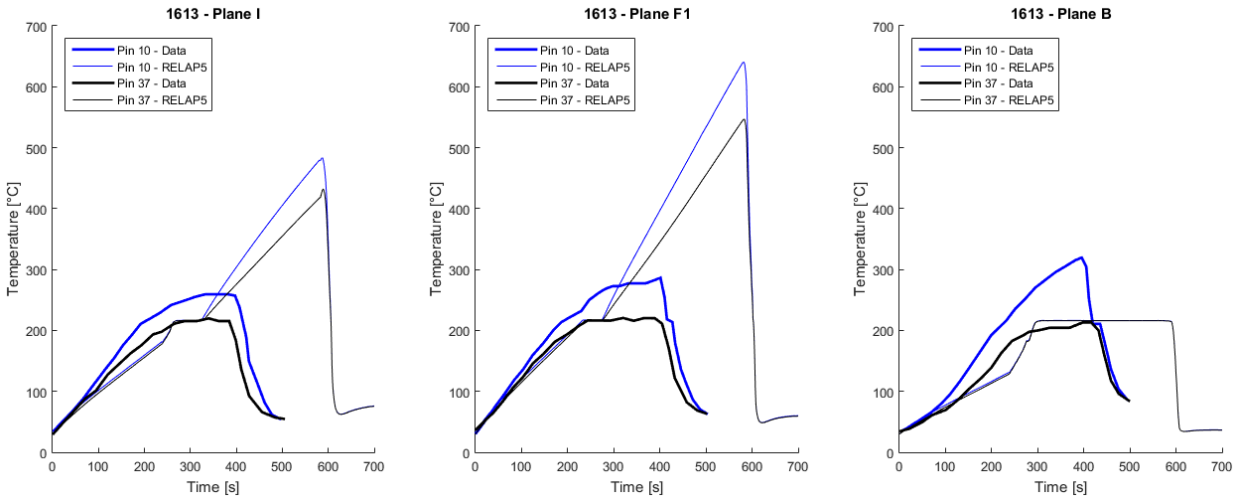

Figure 18 Comparison of experimental and simulated data for sheath temperatures in test 1613

The venting time and maximum fuel temperatures for both the experiment and the simulation are summarized in **Error! Reference source not found.**. It can be seen that the heat transfer between the FES surface and the coolant is modeled fairly well up to approximately $300\ s$ and then there is a shift in the simulated data resulting in near-adiabatic heat up while the pins are exposed to steam. Additionally, the venting time is significantly over-predicted by the current RELAP5 scheme.

Table 5 Venting time and maximum sheath temperature for experimental and simulated results of test 1613

	CWIT Data		**RELAP5 Data**	
	Value	**Location**	**Value**	**Location**
Maximum Sheath Temperature	$319.5℃$	Pin 10 Plane B	$640℃$	Pin 10 Plane F1
Time to Vent	$450\ s$		$600\ s$	

6.5.2 Low Power (Test 1617)

Figure 19 shows the fuel sheath temperature for the low power experiment for pins 10 and 37. Both the CWIT dataset and the RELAP5 dataset are shown.

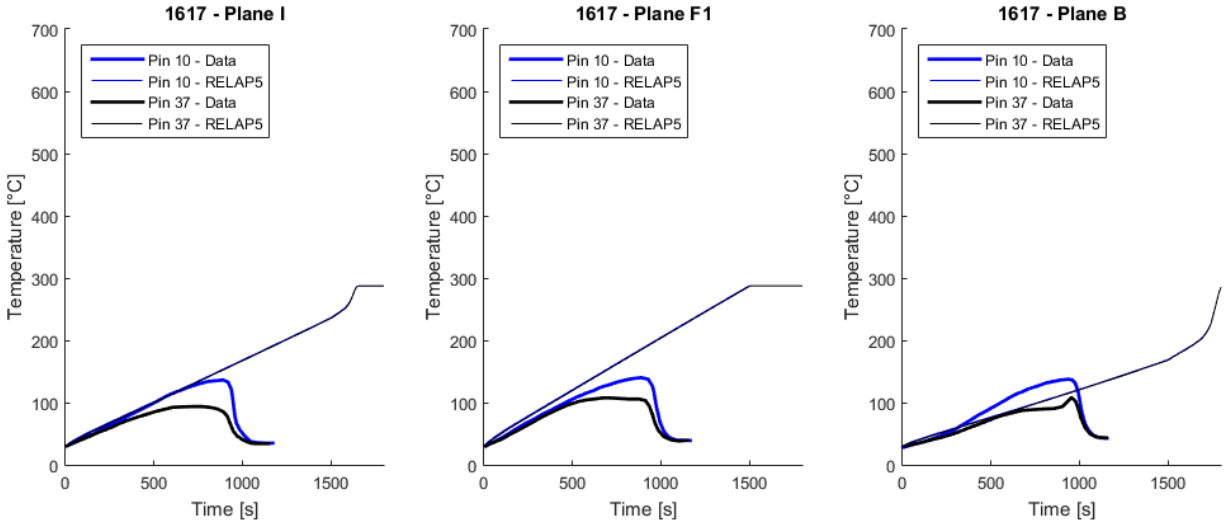

Figure 19 Comparison of experimental and simulated data for sheath temperatures in test 1617

Similar to the high-power case, the maximum fuel temperatures are over-predicted by the RELAP5 simulation. However in this case, the simulated conditions in the channel do not allow for venting to occur. This will be discussed further in Section 8.

7. Sensitivity Studies

The following sections make an effort to assess the sensitivity of the simulated results to the assumptions and nodalization choices made during the creation of the input decks. For this purpose, the high-power experiment was chosen as a reference case. The imposed conditions resulted in full venting of the void, providing an avenue for both a qualitative and quantitative look at the sensitivity of both the venting time and the associated maximum fuel temperature. All results are compared against the reference simulation data for pin 10 (the top of the channel) at plane F1 (the middle of the channel).

7.1 Nodalization Details

7.1.1 K-Factors

Throughout the CWIT facility test loop there are a large number of bends, tee-junctions, orifices, valves and other non-circular geometries for which the minor pressure losses must be explicitly modeled. Each location within the facility was carefully matched with the corresponding junction in the RELAP5 realization of the facility and best-estimates were made for the value of the loss coefficient to be applied. Figure 20 shows the pin 10, plane F1 data for three cases:

1) The best estimate scenario for all implemented k-factors
2) A scenario in which all implemented k-factors were increased by 10%
3) A scenario in which all implemented k-factors were decreased by 10%

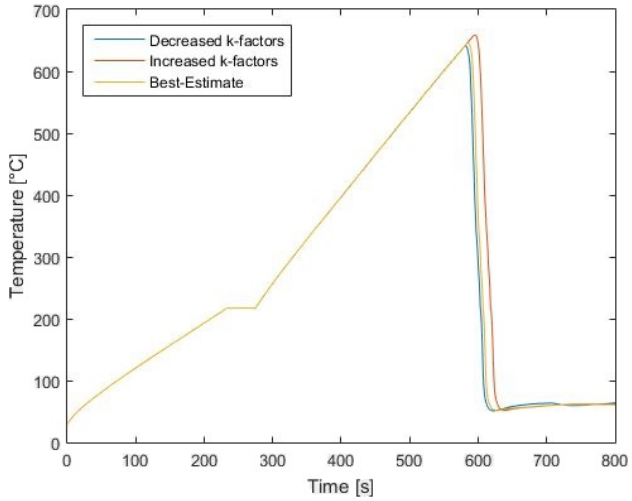

Figure 20 Simulation sensitivity to k-factor values

It can be seen that a decrease in all of the system minor loss coefficients results in a decrease in the venting time and maximum fuel temperature of $4\ s$ and $5℃$ respectively. An increase in the system minor loss coefficients results in an increase in the venting time and maximum fuel temperature of $10\ s$ and $12℃$. The change in venting time falls within a range of $\pm 1\%$ of the reference case venting time and the change in maximum temperature falls within a range of

$\pm 2\%$. Both ranges indicate that the nodalization scheme used for the reference case results are fairly insensitive to the best-estimates of the system minor loss coefficients.

7.1.2 Volume Length and Junction Location Approximations

Figure 8 indicates that the injection lines connect with the headers at an elevation 3” below the central axis of the header. It was initially unclear which face of the header volumes to connect the injection line to in order to accurately capture the thermalhydraulic behaviour of this setup (ie. the bottom face or the side face).

In addition to this, there are several places where the available engineering drawings and associated documentation do not provide all of the information needed to nodalize the facility. One significant example of this is in the total length of the section of feeder pipe that is connected to the header. The total height from the central axis of the header to the first horizontal bend in the feeder pipe is given, but the length of the angled portion is missing. This section of pipe is also shown in several diagrams with significantly different qualitative proportions and so an estimate was required. This type of scenario occurred in several places within the system.

In order to qualify the estimations made, several simulations were run in which these unknown parameters were changed. Figure 21 shows one such simulation where each of the aforementioned estimations were changed to reasonable extremes. It can be seen that the effects of these changes are insignificant.

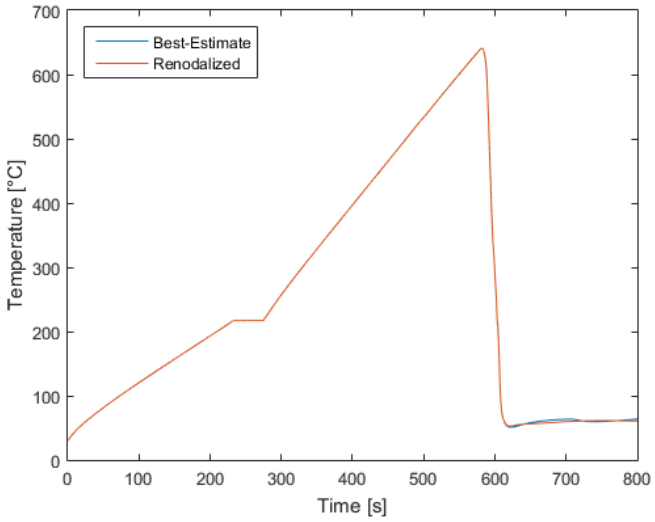

Figure 21 Simulation sensitivity to nodalization estimations

7.1.3 End-Fitting Dead Space

It was discussed in Section 6.1.4 that the CWIT Facility end-fittings do not have the same central dead space that is characteristic of the CANDU end-fitting. The baffle plates used to secure the FES assembly provide a near water-tight seal. Previously performed simulations of the CWIT Facility using GOTHIC [17] assumed a zero-flow condition between the dead space and the transition to the annular flow region. Figure 22 shows a renodalization of the end-fittings that includes a flow path to the dead space. Figure 23 shows the corresponding simulation pin 10 temperature associated with this change.

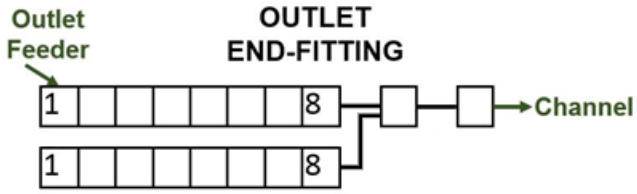

Figure 22 Renodalization of end-fittings to include flow path to dead space

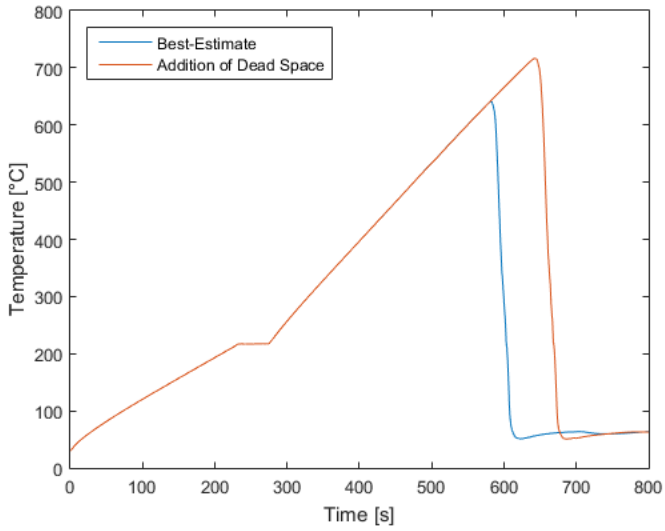

Figure 23 Simulation sensitivity to allowance of flow through the end-fitting dead space

It has been found that the results of the CWIT Facility simulations are most sensitive to the end-fitting nodalization scheme. The addition of flow to the dead space causes an increase in venting time and maximum fuel temperature of ~ 65 s and ~ 80℃ respectively. These increases are over 10% of the reference dataset values and are an indication that the results are fairly sensitive to the way in which the end-fitting is nodalized.

7.1.4 End-Fitting Flow Area

The portion of the end-fitting in which the coolant transitions from the channel geometry to the annular geometry (refer to Figure 9 and Figure 13) was not documented in detail. In particular, the area through which the coolant can flow required estimation. Figure 24 shows the results of a simulation in which the best-estimate for the flow area based on the available information was increased by approximately 20%. The resulting venting time and maximum fuel temperatures were observed to be $\sim 3\ \mathrm{s}$ and $\sim 3℃$ respectively above the reference case. These changes correspond to $< 0.5\%$ of the reference dataset values indicating a very low sensitivity to the flow area of this junction.

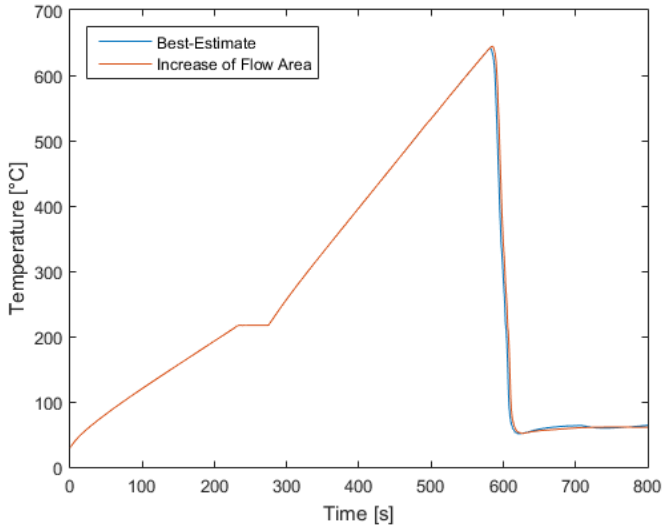

Figure 24 Simulation sensitivity to end-fitting flow area

7.1.5 End-Fitting to Feeder Connection

In addition to the inclusion of dead space and the value of the transitional flow area, the placement of the feeder connection to each end-fitting required some approximation. It can be seen in Figure 8 that the feeder connection is several centimetres from the end of the component. This placement falls close to the junction between volumes 1 and 2 of the finalized end-fitting scheme (Figure 13) and it was consequently unclear initially where to make the connection in the input deck. In the best-estimate reference simulation, the connection was implemented as a crossflow junction on the side face (face 4 in the RELAP5 numbering convention).

Figure 25 shows a comparison of the reference case to cases where the feeder connection was placed at volume 2 (a reasonable placement given the physical setup of the component) and volume 8 (a non-physical placement given the facility drawings, however this placement provides some insight into the problem of the overpredicted venting time and will be discussed further). The change in placement from volume 1 to volume 2 corresponds to $\sim 5\ \mathrm{cm}$ along the

end-fitting and yields a change in venting time and maximum fuel temperature of $\sim 20\ s$ and $\sim 25℃$ respectively. This indicates a fairly high sensitivity to this parameter.

As will be discussed further in Section 8, the time required for the metal in the end-fittings to heat up enough to allow full void penetration along its axis is significant. The default one-dimensional nature of RELAP5 forces average fluid properties on the cross-section of the volumes. It is probable that in the experiments, the vapour and liquid phases experience enough stratification along the axis of the end-fitting that the temperature of the end-fitting metal will be significantly different on the top and the bottom. This would then allow for the void to penetrate along the top of the end-fitting without significant condensation and in turn allow for venting to occur earlier than is observed in the reference simulation. In order to show the effect this would have on the global results, Figure 25 also shows the pin 10 temperature when the feeder is connected to volume 8 of the end-fitting (ie. a volume very close to the channel entrance). The direct consequence of this change is that the time required for the cross-sectional average fluid and metal properties to become favourable for the presence of sufficient venting buoyant force is bypassed. It can be seen that the resulting venting time shown in Figure 25 is very close to the experimental venting time.

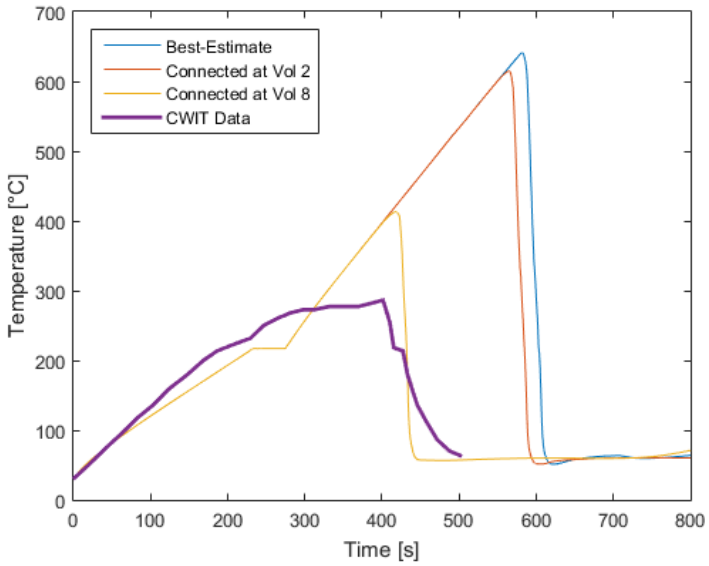

Figure 25 Simulation sensitivity to location of feeder connection to end-fitting

7.2 The CANCHAN Component

The CANCHAN model (in conjunction with convective boundary condition type 124) was compared with the use of the PIPE component in conjunction with the normal horizontal bundle condition type 134. Figure 26 shows the results of this comparison for a volume in the centre of the channel (plane F1) and for both pins 37 (central pin) and 10 (at the top of the channel). The PIPE model predicts significantly higher void generation and subsequent venting through the feeder (even though the venting time and maximum fuel temperatures are over predicted). The CANCHAN model on the other hand does not simulate as much steam production due to the fact that the heat produced by the uncovered pins is transferred entirely to the steam. In the

case of the PIPE component, a portion of the power is directed to the liquid phase, generating more vapour. Since the steam flow to the end-fittings is much less in the CANCHAN simulations, the venting time will occur much later than in the PIPE simulations.

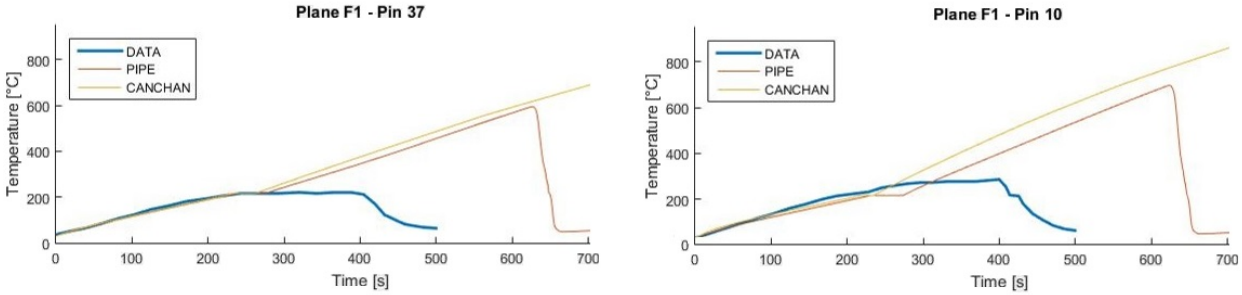

Figure 26 Simulation sensitivity to choice of PIPE versus CANCHAN component in channel

8. Discussion of Results

Figure 27 shows an in-depth look at the relevant channel properties for the high-power experiment. The top row shows the fuel sheath temperature data for both the experiment and the reference simulation for three planes along the axis of the channel. The middle row shows the void fraction as a function of time within the corresponding planes. The bottom row shows both the flow regime (red) and the wall-to-fluid heat transfer regimes (blue and black) for the corresponding planes. As was discussed in Section 6.5.1, RELAP5 overpredicts both the venting time and the maximum fuel temperatures for this experiment.

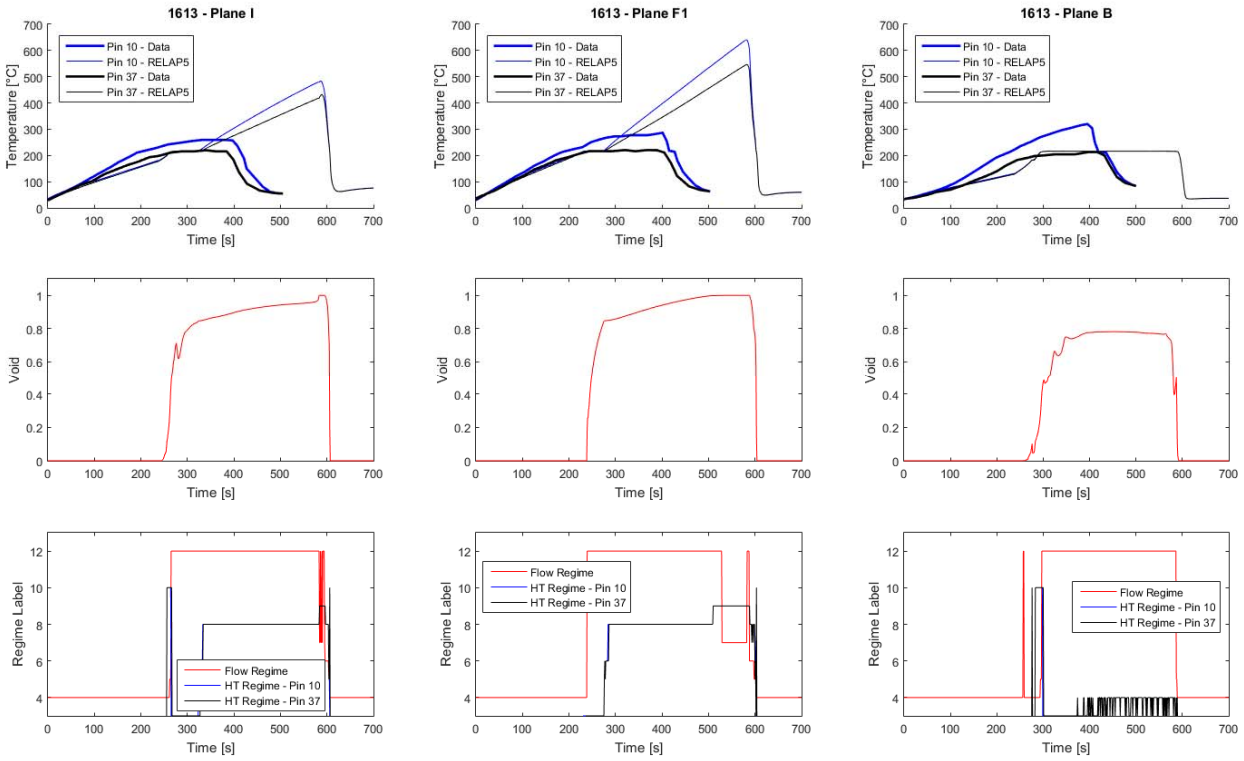

Figure 27 Channel properties for the simulation of test 1613

The overprediction of fuel temperature can be explained by an improper assignment of heat transfer coefficients under these conditions. The point in time at which the pin temperatures take off corresponds to the transition from BBY to HST flow. With the use of the PIPE component, there is no height assignment to the heat structures and the occurrence of HST flow implies only that a different set a cross-sectional average fluid conditions be generated. In reality however, there is a layer of boiling fluid at the bottom of the pipe with lateral movement across the fuel elements, a non-static interface geometry and a layer of steam at the top of the pipe with a high level of liquid entrainment. The heat transfer coefficients required to model these conditions accurately would be much higher than the near adiabatic behaviour observed in the simulated results. This implies that new heat transfer correlations would need to be implemented within the RELAP5 source code for more accurate modelling of the wall-to-fluid heat transfer during stagnant, stratified flow conditions in a horizontal fuel channel.

The overprediction of the venting time is heavily dependent on the nodalization of the end-fittings (as discussed briefly in Section 7.1.5). To illustrate this further, Figure 28 shows the void fraction at several locations around the end-fittings for the high-power simulation. In this simulation, the void vents through the outlet side as indicated by the short pulse of 100% void in several locations along the outlet end-fitting. It can be seen that the void begins to penetrate the end-fitting at approximately $400\ s$ (the time at which the experimental data indicates venting), quickly rises to a value of $\sim 30\%$ and plateaus at this value for over $100\ s$. During this time, the metal in the end-fitting is heating up and the steam is continuously condensing. RELAP5 does not explicitly model the stratification that is occurring in the stagnant fluid of the end-fitting. There should be liquid on the bottom and superheated steam in a layer along the top. This in

turn should yield a buoyancy force for the steam that is much higher than that based on the cross-sectional average void calculated by RELAP5.

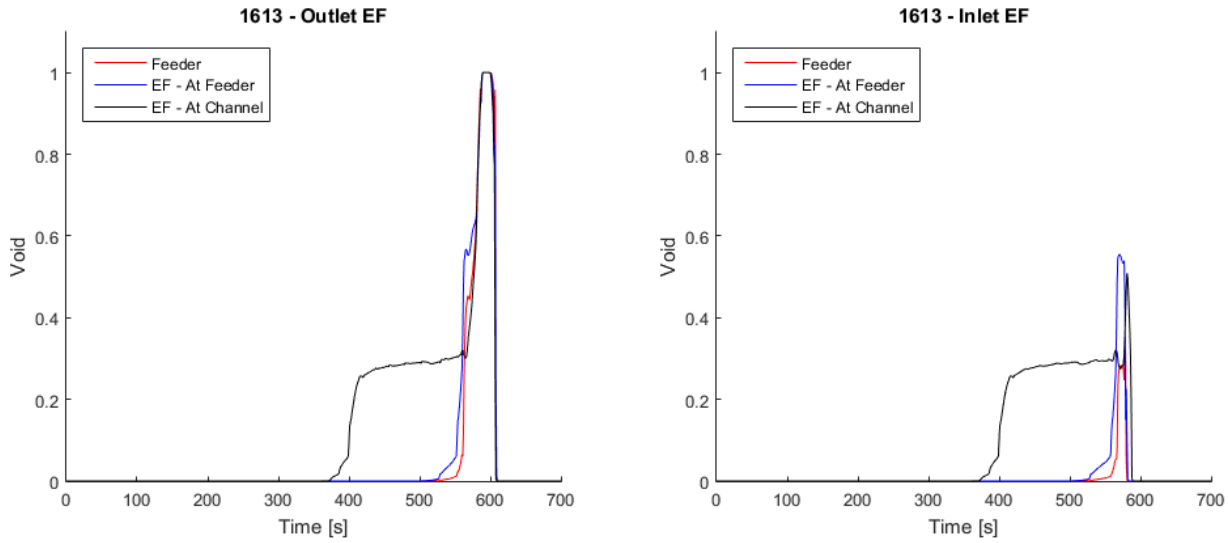

Figure 28 Void fraction along end-fittings for simulation of 1613

It takes approximately $200\ s$ for the end-fitting material to rise to a temperature sufficient to reduce condensation and allow for the volume-averaged density to be enough to overcome the elevation head and permit venting to occur. In the experimental facility, the stratified conditions with superheated steam along the length of the end-fitting will allow a higher void fraction at the feeder connection much sooner than is observed in the simulation. Figure 29 shows a further look into this issue with the void fraction at several planes (along the top) and the end-fitting metal temperature, fluid temperature and saturation temperature for the corresponding planes.

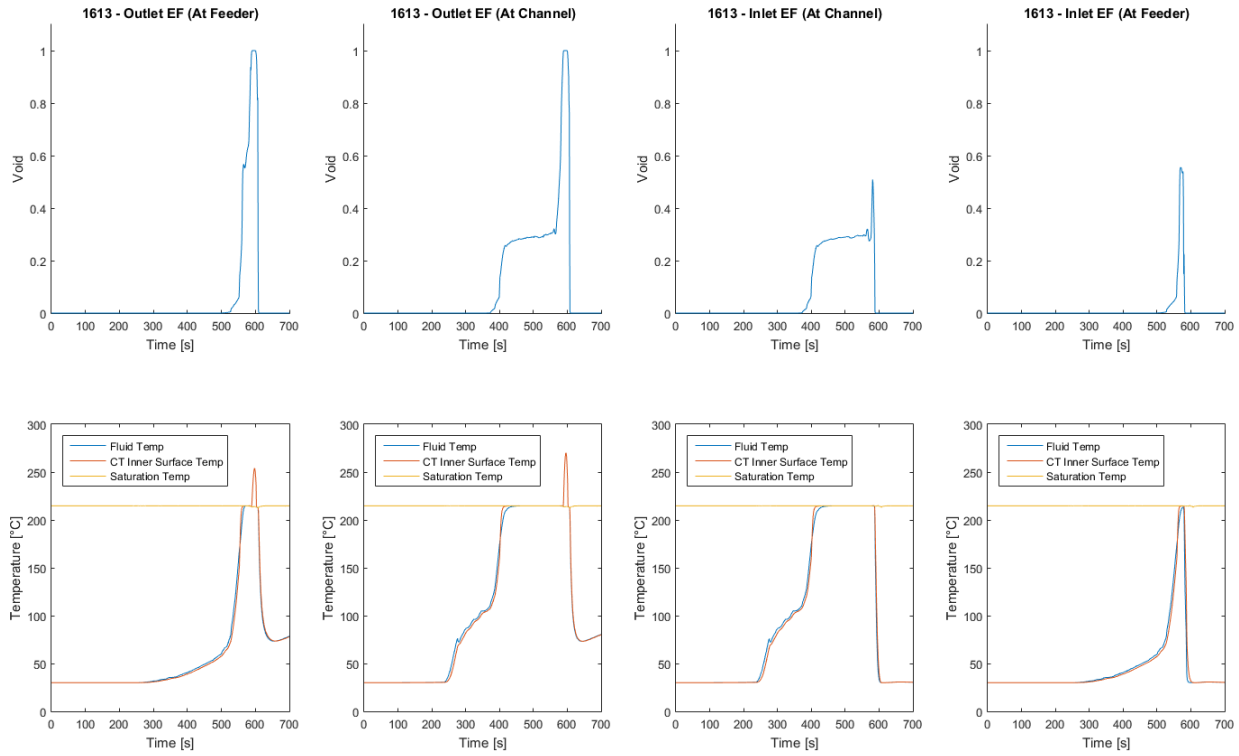

Figure 29 End-fitting properties for simulation 1613

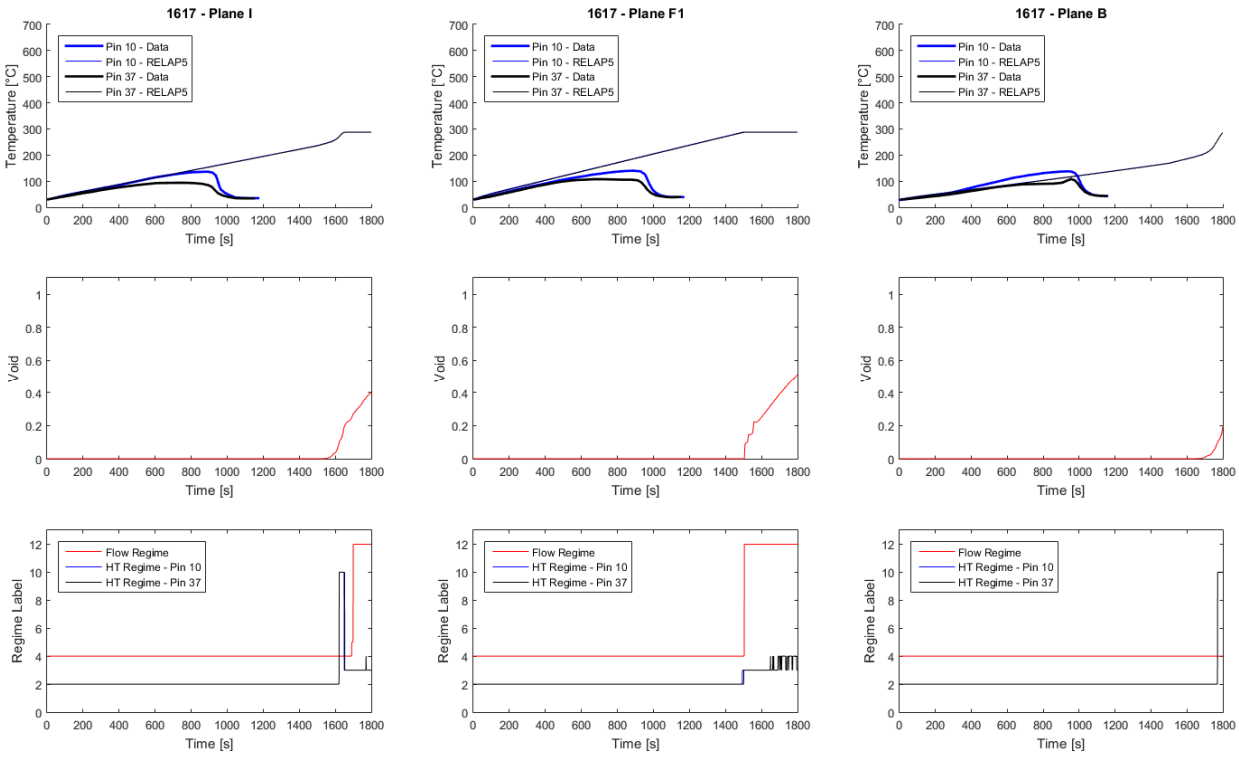

Figure 30 Channel properties for the simulation of test 1617

Figure 30 shows the same parameters along selected planes of the channel for the low power experiment. Reference [17] states that this test in the standing start series was chosen due to the fact that it vented in single phase. Figure 30 shows good agreement between the experimental and simulated pin temperatures for approximately 800-1000s at which point venting in the experiment occurs.

It has been documented that the quenching behavior of the top and bottom half of the end-fittings is different in some of the tests. Consequently it is possible that the liquid level during stratified conditions can play as important a role as it does in the channel with regard to the determination of the wall-to-fluid heat transfer coefficient. Several alternate approaches to the nodalization scheme will be implemented in order to study the sensitivity of the local and global results to the nodalization scheme. If the CANCHAN component with heat structure elevations proves to accurately model the channel heat transfer conditions, it is possible that this component can be used in the end-fittings as well. It is also possible to split the flow path into layers and separately model the upper and lower sections of fitting with crossflow connections applied in the vertical direction between the layers (refer to Figure 5). Such changes may require source code modifications beyond the scope of this project.

9. Conclusions

The RELAP5 code is an excellent generic system thermalhydraulic code capable of simulating a wide range of transients in LWR and CANDU reactor designs. This work provides a thorough investigation of the models and predictive capability of the RELAP code in simulating the CANDU specific phenomena involved in IBIF. Based on this we conclude:

- RELAP5 does simulate all the relevant phenomena and does predict IBIF like behaviour, albeit it over estimates the venting time and sheath/pressure tube temperatures significantly.
- Under nearly stagnant conditions in an IBIF, RELAP applies a steam heat transfer coefficient to pins above the water line. While this seems appropriate, pure steam at zero velocity means that the steam will quickly become superheated and the pins will almost adiabatically heat up (since the flow is near zero). In reality there will be vigorous boiling from the submersed pins which will act to i) add some moisture content to the steam above the water line, lowering the amount of sensible heat to the steam and ii) cause better than adiabatic heat transfer from the pins. Such phenomena is supported by the CWIT experiments that show pins above the water line tend to plateau and not increase unbounded after uncovery.
- Using any option in RELAP (either CANCHAN or PIPE) for the channel, steam is generated in the center of the channel and through condensation at the end fitting acts to heat up the end fitting. Eventually void penetrates far enough into the end fitting body such that it reaches the feeder connection, and in RELAP this shows up as a gradual increase in the void fraction in the end fitting nodes. However despite our best efforts the penetration of the void to the feeder connection is not modelled adequately because there is no comparable stratification model for the end fitting, only for the channel in CANCHAN. In reality there exists a high void fraction (or steam) region at the top of the end fitting and low void fraction at the bottom, and RELAP is unable to easily handle this segregation. Since RELAP does not explicitly model this stratification the vapour penetration at the feeder connection it under predicts the buoyancy force, and hence venting times are significantly longer than the experiment.

10. References

[1] P. I. a. J. Luxat, Natural Circulation in and Integral CANDU Test Facility, IAEA-TECDOC-1149, 2000.

[2] C. M. a. J. Wedgewood, Description of the Cold Water Injection Test Facility, COG File COG-96255, 1996.

[3] Z. K. a. M. Kawaji, A Study of Intermittent Bouyancy Induced Flow Phenomena in CANDU Fuel Channels, NURETH 13, 2009.

[4] J. A. A. M. a. R. L. P. Wan, Some Ideas of Thermosyphoning in a Heat Transport Loop, AECL Report.

[5] Q. Lei and P. Gulshani, "Assessment of Fuel Fitness-for-Service After Standing Start Process Under Gentilly 2 Shutdown Conditions," in *19th Annual CNS Conference*, 1998.

[6] J. Spencer, "Analysis of Intermittent Buoyancy Induced Flow in Asymmetrically Obstructed CANDU Nuclear Fuel Channels," McMaster University, Hamilton, Ontario, 2010.

[7] I. S. L. Inc, "RELAP3.3 MOD3.3 Code Manual Volume IV: Models and Correlations," Idaho Falls, Idaho, 2016.

[8] J. Chen, "A Correlation for Boiling Heat Transfer to Saturated Fluids in Convective Flow," proc Des Dev Vol 5., 1966.

[9] R. S. F. O. J.C. Chen, "A Phenomenological Correlation for Post CHF Heat Transfer," NUREG-0237, 1977.

[10] L. Bromley, "Heat Transfer in Stable Film Boiling," Chem Eng Progress, Vol 46, 1950.

[11] e. a. K.H. Sun, "Calcualtions of Combined Radiation and Convection heat Transfer in Rod Bundles Under Emergency Core Cooling Conditions," J. of Heat Transfer,, 1976.

[12] S. C. a. T. D. D.C. Groeneveld, "1986 AECL-UO Critical heat Flux Lookup Table," Heat Transfer Eng. Vol. 7, 1986.

[13] J. Sellars, M. Tribus and J. Klein, "Heat Transfer to Laminar Flows in a Round Tube or Flat Conduit: The Graetz Problem Extended," *Transactions, American Society of Mechanical Engineers,* vol. 78, p. 441, 1956.

[14] F. Dittus and L. Boelter, "Heat Transfer in Automobile Radiators of the Tubular Type," *Publications in Engineering, University of California,* pp. 443-461, 1930.

[15] W. H. McAdams, Heat Transmission, New York: McGraw-Hill, 1954.

[16] K. Shin, "Data Report for Standing Start Tests Conducted with the West Channel in the Cold Water Injection Test Facility," Stern Laboratories and Ontario Power Generation, 2001.

[17] J. Spencer, "Analysis of Intermittent Buoyancy Induced Flow in Asymmetrically Obstructed CANDU Nuclear Reactor Fuel Channels," McMaster Univeristy, Hamilton, Ontario, 2010.

[18] Y. Taitel and A. E. Dukler, "A Model of Predicting Flow Regime Transitions in Horizontal and Near Horizontal Gas-Liquid Flow," *AIChE Journal,* vol. 22, pp. 47-55, 1976.